Chapter 4

MODELS OF GAP DETECTION IN ELECTRIC HEARING

1 INTRODUCTION

Gap detection is often employed as a way to probe the temporal resolution ability of the auditory system (Shannon, 1989). Gap detection thresholds in electrical stimulation were measured by Shannon (1983a), Preece and Tyler (1989), Shannon (1989), Hanekom and Shannon (1998), Chatterjee, Fu, and Shannon (1998), Busby and Clark (1999) and Van Wieringen and Wouters (1999) under various conditions.

Shannon (1989) measured gap detection as a function of intensity of stimulation, using sinusoids and pulse trains, with both gap markers presented on the same electrode pair (a within-channel condition). He found that gap thresholds are a strong function of stimulus level, with longest gap thresholds of more than 50 ms (at near audible threshold stimulation levels), and shortest gap thresholds of less than 1 ms (at high stimulation levels).

Preece and Tyler (1989), who measured gap detection thresholds in cochlear implants using sinusoidal electrical stimulation, ascribed the longer gap thresholds at lower stimulation levels to a decay of sensation theory of gap detection (Penner, 1977). According to this theory, the gap is detectable when the sensation has decayed by a just-noticeable amount, or when the signal level has changed by more than the intensity difference limen, which is larger near auditory threshold.

Although neural synchrony is much higher in biphasic electrical stimulation than in acoustic stimulation (Javel, 1990) and differs in the pattern and extent of activated nerve fibres (Kral

et al., 1998), Shannon (1989) showed that electrical and acoustic stimulation produced similar gap detection performance. This suggests that gap thresholds are not primarily determined by temporal processing of individual fibre spike trains.

Hanekom and Shannon (1998) employed gap detection, not as a measure of temporal resolution, but as a way to measure electrode interaction in cochlear implants (see chapter 2). The hypothesis was that if the two gap markers were presented on different electrode pairs, gap thresholds would be small when the two electrode pairs stimulated the same neural population (a within-channel condition), and would increase as the neural populations became more disjunct (an across-channel condition; electrode interaction becomes less). If this hypothesis is true, the pattern of gap thresholds as a function of distance between the two marker electrode pairs will also reflect the current distribution in the cochlea. This suggests that one should be able to estimate the current distribution pattern in the cochlea from gap detection tuning curves.

Chatterjee et al. (1998) argued that the U-shaped curves achieved by Hanekom and Shannon (1998) (see chapter 2) could be attributed to a perceptual discontinuity, rather than reflecting the amount by which stimulated neural populations overlap (an across-channel mechanism). They showed that U-shaped curves can also be obtained with a within-channel gap detection mechanism, by presenting both gap markers on the same electrode, but using different stimulation pulse rate or intensity of stimulation for the two markers. Busby and Clark (1999) showed that rate of stimulation (pulse rates of 200 pps, 500 pps and 1000 pps were used) does not influence gap thresholds when the rate of stimulation is the same on both markers.

Van Wieringen and Wouters (1999) measured gap detection thresholds in users of the LAURA cochlear implant. They measured gap detection thresholds in various within-channel and across-channel conditions. Not all of their data showed an effect of distance between electrode pairs when pre- and post-gap markers were presented on different electrode pairs (as was found in Hanekom and Shannon (1998)) and, furthermore, a strong effect of training was found. It appeared that once subjects had been trained to attend to the gap in the presence of

confounding factors, the effect of distance between pre- and post-gap electrode pairs disappeared in some subjects. A primary interpretation of their results was that gap detection thresholds depend more on the subject's inability to attend to the gap when confounding factors are present than on neural interaction. Finally, it is noted that, as in most cochlear implant psychoacoustics studies, the subjects in the Van Wieringen and Wouters study showed much inter-subject variability.

The poorer gap detection performance in acoustic across-channel experiments has been attributed to an auditory attentional process (Phillips et al., 2000). These authors proposed that two different mechanisms operate in within-channel and across-channel gap detection tasks. For within-channel gap detection (in cochlear implants, this is when both markers are presented on the same electrode pair), the task of the auditory system is to detect a discontinuity. In across-channel gap detection (in cochlear implants, this is when markers are presented on different electrode pairs that stimulate disjunct or overlapping but non-identical neural populations), the discontinuity always exists. The task now becomes one of gap duration discrimination. The authors speculated that (in across-channel gap detection) attention resources are allocated to the first marker, resulting in deteriorated ability to measure the time interval between the two markers. A related idea, expanded on later, is employed in the current model. It should be noted that Oxenham (2000) provides reasonable arguments against the idea that attention resources are loaded to the extent that gap detection ability deteriorates.

1.1 Information available to the central detector in acoustic and electric gap detection

1.1.1 Temporal response properties

Two major differences exist in the information available to the central detector in acoustic and electric gap detection. First, in acoustic gap detection, spike trains are much more Poissonian in nature than the highly entrained spike trains found in electric gap detection. This is especially true for acoustic gap detection employing bandlimited noise markers (as used in e.g. Phillips et al. (2000)). Spikes may also occur during the gap, which is seldom the case in electric

hearing (Shepherd and Javel, 1997), as spontaneous activity is usually not present in the deafened auditory system. In the acoustic gap detection situation, the central gap detector probably has to base decisions on the envelope of the marker-gap-marker auditory event as reflected in spatially distributed neural spike train patterns, rather than on individual inter-spike intervals. As explained below, it is likely that the gap detector bases its decisions on inter-spike intervals in electric hearing.

Phase locking of spike trains to the stimuli, similar to what happens in electric hearing, occurs (below 5 kHz, Johnson, 1980) in acoustic gap detection experiments using sinusoidal markers (e.g. Formby and Forrest, 1991). However, 100% entrainment (spikes occur in response to each stimulus pulse) to the preferred stimulus phase as is found in electrical stimulation (Javel, 1990) seldom occurs in acoustic stimulation (Rose et al., 1968). 100% entrainment in pulsatile electrical stimulation can occur at pulse repetition frequencies of up to 800 Hz for healthy or short-term deaf ears, but the ability to entrain to high frequencies is reduced in long-term deafness. Shepherd and Javel (1997) observed entrainment only up to 400 pps in long-term deaf fibres. This is probably a result of prolonged refractory periods that occur in nerve fibres that are demyelinating (Shepherd and Javel, 1997).

Spike position jitter relative to a preferred latency (following a stimulus pulse) has significantly larger standard deviation in acoustic stimulation (Javel and Mott, 1988) than in electrical stimulation (Javel and Shepherd, 2000). Spike position jitter increases with higher frequency in electrical stimulation (Javel, 1990; Javel and Shepherd, 2000), but decreases in acoustic stimulation (Javel and Mott, 1988).

Different response types may be evoked in response to an electric stimulus pulse. As shown in Javel and Shepherd (2000) and Javel (1990), spikes that occur in response to electrical pulse stimuli, cluster into one of four discrete latency windows. These have been labelled *A*, *B*, *C* and *D* responses, in order of increasing latency. Different spike latencies probably result from spike initiation at multiple sites. *A* responses have short latency (in response to the stimulus pulse) and have small temporal jitter. *B* responses have longer latency and more spike position jitter.

Both *A* and *B* responses are observed in deafened ears, but the *A* response is predominant. Just *A* responses are often observed in the majority of fibres in long-term deaf ears (Shepherd and Javel, 1997).

D responses occur with long latency and are not observed in deaf animals and are therefore not relevant to cochlear implants. The *C* response is primarily found at near-threshold intensities, and is possibly just a near-threshold extension of the *B* response. This response probably arises from spikes initiated at the peripheral processes of the spiral ganglion cells. The short latency *A* response probably results from spikes initiated at the central processes of spiral ganglion cells. Latency transitions from *B* to *A* responses are sometimes observed as stimulus intensity is increased, but this transition is not found in long-term deaf ears (Shepherd and Javel, 1997). Van den Honert and Stypulkowski (1987a) observed that both phases of a biphasic pulse stimulus can elicit spikes and that these spikes may be initiated at different sites, and therefore with different latencies. *A* and *B* responses may result from different phases of a biphasic stimulus pulse.

1.1.2 Spatial excitation patterns

The second difference between acoustic and electric gap detection is that a wider extent of neural activation is brought about with electrical stimulation. Maximum slopes of spatial tuning curves of 8 dB/mm have been measured for bipolar electrical stimulation with the Nucleus electrode array (Kral et al., 1998), while tuning curves in the 8 kHz region can have slopes of up to 100 dB/mm in acoustic stimulation. Furthermore, current spread may increase in long-term deafness, due to demyelination of nerve fibres (and therefore changing resistive pathways) (Shepherd and Javel, 1997).

In summary, in electric gap detection a wide spatial extent of spike trains, weakly to highly entrained to the stimulus pulse train, contains the gap. The area of activation is narrower in acoustic gap detection and the gap is contained in much noisier spike trains.

1.2 Differences in the gap detection task between acoustic and electric hearing

Although the neural circuitry of the central detector will be the same in both cases, the task of the central detector in electric and acoustic gap detection is probably different. As discussed before, the within-channel gap detection task in acoustic stimulation is one of detection of a transition. The across-channel gap detection task is a time duration discrimination task, with gap detectability limited by (i) the masking of edges of the gap as a result of Poisson encoding, and (ii) the measurement accuracy of the "Poissonian timer" (see chapter 3).

When entrainment is 100% in electrical stimulation, the task is to detect one slightly longer inter-spike interval within a series of fixed duration inter-spike intervals observed with high signal to noise ratio (the noise being the spike position jitter). This is a classical detection task.

When entrainment is less than 100%, the real gap is hidden by spike trains containing "gaps" that are multiples of the stimulation pulse repetition period. Detecting the actual gap when it is small (a fraction of one pulse period for 100% entrainment) will be quite difficult for a detector by observing a spike train from just a single fibre. In this case, the gap will have to be longer than the typical inter-spike intervals obtained when entrainment is 100%. This notion will be explained in more precise terms later.

In both cases (100% entrainment or less) in electric hearing, the detector will need to compare each inter-spike interval against a threshold. Accurate measurement of the inter-spike interval is not required. So it seems the task in gap detection in electric hearing does not reduce to a duration measurement task in the across-channel condition.

1.3 Models for gap detection

Several models for gap detection in acoustic hearing were discussed in the previous chapter. As far as is known, no previous models of gap detection in electric hearing exist. An appropriate model for gap detection should be able to predict (i) the sensitivity of gap detection

thresholds to intensity of stimulation as found by Shannon (1989), (ii) the U-shaped curves found by Hanekom and Shannon (1998) and Chatterjee, Fu, and Shannon (1998) (under different conditions) and (iii) the correct magnitude of gap detection thresholds as found by several authors. Such a model should employ a biologically plausible mechanism and plausible parameter values.

Two possible mechanisms, or a combination thereof, may be adopted to explain gap detection thresholds. The first explanation is primarily based on temporal mechanisms. It has been hypothesized that ringing in the mechanical response of the basilar membrane following stimulus offset prolongs the neural response, so that these spikes will tend to fill the gap (Zhang et al. 1990).

Cochlear implants stimulate nerve fibres in the cochlea directly, so that the cochlear filtering step is bypassed. Neural synchronization is high, with 100% entrainment of neural spike trains to the stimulation pulses often occurring in fibres close to the electrodes (Javel, 1990), and generally no neural activity occurring when the stimulus is absent. Improved gap detection thresholds might reasonably have been expected for electrical stimulation of the auditory system. However, evidence suggests that gap detection thresholds do not depend on neural synchronization alone (Shannon, 1989), and that other sources of noise affect the ability of the central gap detection mechanism to detect the presence of the gap accurately.

A second possible explanation of gap detection thresholds in cochlear implants lies in the mechanism of "auditory attention". This is a spatial, rather than temporal, mechanism. The hypothesis is that the auditory system can only attend to a limited spatial extent of neural activity. Accordingly, an idea related to the auditory attention mechanism suggested by Phillips et al. (2000) is employed in the current model. The model proposes that the *detectability* of the second marker onset deteriorates when the marker electrode pairs are moved apart. In contrast to the explanation of Phillips et al. (2000), no time measurement is required in the model.

It is implicitly assumed that the listener attends to the gap in the gap detection task. Taking a neurophysiological view, it is assumed that attention in this case means that the central detector observes a spatially limited extent of fibres. To detect the gap, it is necessary that the detector observes a set of fibres with spike trains entrained (not necessarily 100%) to *both* the gap markers. If this is not so, the central detector would either observe the offset of the pre-gap marker, or the onset of the post-gap marker, and the gap will not be detected. The limited extent of fibres observed will consequently probably be situated somewhere midway between the two electrode pairs defining the two markers. When the marker electrodes are far apart, the observation window will contain fibres with low entrainment.

This attentional mechanism is explored in this chapter. It is emphasized that this is a viewpoint that is based on unproved assumptions.

1.4 Objectives of this chapter

In summary, this chapter intends to build understanding of the processes underlying the results achieved in the psychoacoustics of gap detection in electric hearing, by creating models that can predict the data reported in chapter 2. It is shown that gap detection data can be predicted by a model that uses cochlear spatial information, using plausible model parameters. Accordingly, gap detection ability does not necessarily reflect temporal processing mechanisms. The model hinges on the idea that a spatially limited neural observation window is available to a central detector. A final and important result in this chapter is the estimation of current distribution profiles in the cochlea from psychoacoustic gap detection data.

2 A MODEL FOR GAP DETECTION IN ELECTRIC HEARING

2.1 Assumptions about the electrically evoked spike train

The model assumes a long-term deaf auditory system. Consequently, it is assumed that spikes

are highly entrained to the stimulus pulse train and that only *A* responses occur. This last assumption is motivated by the fact that responses other than the short latency, small jitter *A* responses are seldom observed in electrically stimulated long-term deaf ears. The assumption is made to simplify the model so that obtaining analytical predictions for gap thresholds without reverting to time-consuming (and sometimes less enlightening) Monte Carlo simulation techniques is possible. It would, however, be possible to incorporate "noisier" spike train models (that include *B* and *C* latency responses as well) in a numerical model.

2.2 General formulation of a gap detection model for electric hearing

In a general formulation, the gap detection problem in electric hearing is similar to the acoustic gap detection problem, where (for sinusoidal markers of low frequency) spike trains are phase-locked to the stimulus. 100% entrainment is assumed in this treatment. So it is assumed that spikes occur in response to each marker stimulus pulse with some temporal dispersion (or jitter) and that spontaneous discharges occur during the gap. The average spike rates λ_1 and λ_3 during the markers differ in this general formulation, and they also differ from the average spike rate λ_2 in the gap. To simplify the formulation, it is assumed that spontaneous discharges during the gap do not occur randomly, but rather that these discharges are periodic. Spike position standard deviation is σ_{s1} during the markers, and σ_{s2} during the gap. Figure 4.1 visualizes the spike train model for this formulation.

The optimal detector for an a priori known signal is a matched filter. In the gap detection problem, the "known signal" is the expected transition in spike rate that will occur when the gap occurs. Ideally, the matched filter will know the spike rate during the gap and during each marker. The matched filter for the first transition is shown in figure 4.1(e). If more samples are available, the matched filter detection probability will improve. It is assumed that the signal samples that the matched filter operates on are the inter-spike intervals. The matched filter in figure 4.1 observes the spike train for a time 2T. Assume that N inter-spike intervals are observed in T.

If T is too short, the gap will not be detected. The shortest T for which the percentage of correct transition detections is 76% (d'=1), is the "transition threshold". This threshold will depend on how much λ_1 and λ_2 differ. Both transitions (pre-gap marker to gap, and gap to post-gap marker) need to be detected to detect the gap. The gap will be detected if two consecutive transitions are detected with d'=1.6 as explained in chapter 3.

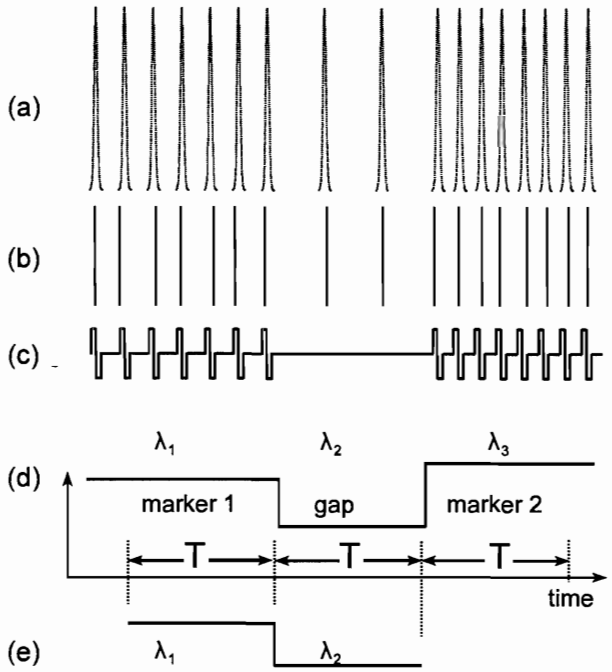

Figure 4.1

This figure gives a general model for the gap detection problem in electric hearing. The progression from the first marker with spike rate λ_1, through the gap with spike rate λ_2, to the second marker with spike rate λ_3 is depicted in (d). The stimulus (gap-marker-gap) is shown in (c). The matched filter shape is shown in (e). (a) shows the distribution of spikes around the preferred stimulus latency. The resulting spike train is shown in (b).

If just one sample (one inter-spike interval) is observed, the detectability is

$$d' = \sqrt{\frac{2(\mu_2 - \mu_1)^2}{\sigma_1^2 + \sigma_2^2}} = \sqrt{\frac{2(\mu_2 - \mu_1)^2}{2\sigma_{s_1}^2 + 2\sigma_{s_2}^2}} = \sqrt{\frac{(\mu_2 - \mu_1)^2}{\sigma_{s_1}^2 + \sigma_{s_2}^2}}. \qquad (4.1)$$

with $\mu_1=1/\lambda_1$ and $\mu_2=1/\lambda_2$, where λ_1 and λ_2 are the spike rate during the first marker and gap respectively. σ_1 and σ_2 are the standard deviations of samples during the marker and gap respectively. The standard deviation σ of a sample is the standard deviation in an inter-spike interval, which is $2\sigma_s$, where σ_s is the spike position standard deviation. σ_{s1} is the standard deviation during a marker, and σ_{s2} during the gap.

If T is longer, so that N samples are observed in T, detectability improves with the square root of N,

$$d'_N = \sqrt{N}d', \tag{4.2}$$

(Green and Swets, 1966). Hence,

$$d'_N = \sqrt{N}\sqrt{\frac{(\mu_2 - \mu_1)^2}{\sigma_{s_1}^2 + \sigma_{s_2}^2}}. \tag{4.3}$$

The number of samples in T is

$$\lambda T - 1, \tag{4.4}$$

where λ is λ_1 or λ_2. The detectability is then

$$d'_N = \sqrt{\lambda_2 T - 1}\sqrt{\frac{(\frac{1}{\lambda_2} - \frac{1}{\lambda_1})^2}{\sigma_{s_1}^2 + \sigma_{s_2}^2}}, \tag{4.5}$$

where λ_2 was used in the expression for N, because it is assumed that $\lambda_2 < \lambda_1$, which implies that spike rate λ_2 during the gap is the critical factor that will determine smallest detectability.

For detection of the gap (detection of two transitions), $d'_N=1.6$ and equation 4.5 is solved for T,

$$T = \frac{1}{\lambda_2} + \frac{\sigma_{s_1}^2 + \sigma_{s_2}^2}{\left(\frac{1}{\lambda_2} - \frac{1}{\lambda_1}\right)^2} \cdot \frac{1.6^2}{\lambda_2}. \tag{4.6}$$

This T is the shortest T that the matched filter will require to detect the gap with at least 76% probability. When the spike standard deviations σ_{s1} and σ_{s1} are small,

$$T \approx \frac{1}{\lambda_2}. \tag{4.7}$$

The minimum value of T is $1/\lambda_2$. Therefore, for small spike jitter (as obtained in pulsatile electrical stimulation), this shows that the matched filter does not require the observation of several stimulation pulses, but will be able to detect the gap by comparing just two inter-pulse intervals (as reflected in the inter-spike intervals), i.e. one interval that does not contain the gap, and one longer interval that does contain the gap.

The gap detection problem can then be reformulated as in figure 4.2. If the duration of the interval that contains the gap is $1/\lambda_2$,

$$\begin{aligned} \textit{gap threshold} &= T - \frac{1}{\lambda_2} \\ &= \frac{\sigma_{s_1}^2 + \sigma_{s_2}^2}{(\frac{1}{\lambda_2} - \frac{1}{\lambda_1})^2} \cdot \frac{1.6^2}{\lambda_2}, \end{aligned} \tag{4.8}$$

which is the gap threshold if the detector searches for two transitions.

2.3 Gap detection model structure for electric hearing

The gap detection problem for electric hearing is depicted in figure 4.2. Having proven that the gap detector only needs to compare each observed sample (inter-spike interval) with the standard inter-spike interval, the task of the detector simplifies to the detection of one longer inter-pulse interval embedded in a pulse train with fixed period (1 ms in this case). The detector does not need to search for two transitions, but just for the longer interval, so that the gap threshold is not given by equation 4.8, but by equation 4.11 below. The gap threshold is taken as the additional time added to the standard stimulus period, when this longer interval is just detectable (76% correct decision in a 2IFC experiment).

2.3.1 Gap detection based on a single fibre when entrainment is 100%

In the experiments modelled here, the stimulation pulse repetition frequency is always the same on both markers. In the simplest scenario, the pre- and post-gap markers are presented to the same electrode pair (the within-channel condition) and the input to the central detector is a spike train on a single nerve fibre. In this scenario, the input to the central gap detector is a spike train that is ideally 100% entrained to the stimulation pulse train with only a small amount of spike position jitter.

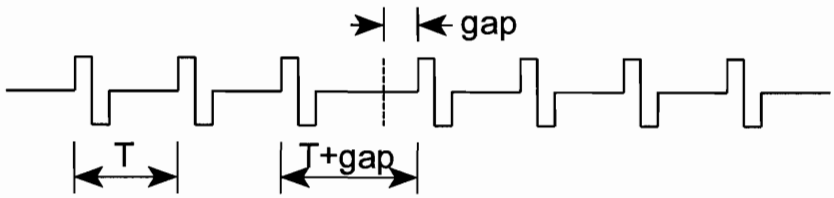

Figure 4.2

A part of a stimulation pulse train with pulse repetition frequency 1/T, showing the definition of the gap.

In this situation, the gap detection problem reduces to a simple signal detection problem: the central detector has to decide which of two inter-pulse intervals occurred, the standard, or the probe (standard plus gap). For this problem, d' is given as

$$d' = \sqrt{\frac{(\mu_1 - \mu_2)^2}{\sigma_{s_1}^2 + \sigma_{s_2}^2}}, \tag{4.9}$$

with $\mu_1=1/\lambda_1$ and $\mu_2=1/\lambda_2$, where λ_1 and λ_2 are the spike rate during a marker and during the gap respectively. For 100% entrainment, the spike rate λ_1 equals the stimulus rate.

Note that in general spikes may occur during the gap, with the spike rate during the gap being λ_2. It was, however, shown in the previous paragraph that under ideal circumstances, when spikes occur only on stimulus pulses (with 100% entrainment), the window T required to detect a gap is equal to $1/\lambda_2$ plus a small duration that is determined by the spike jitter (spike position standard deviation, σ_s). Hence, for 100% entrainment, the temporal window T

required to detect a gap is just slightly longer than the pulse repetition period, so that the detection problem in figure 4.2 is obtained. The detector does not have a large number of samples (inter-spike intervals) in the gap to compare with inter-spike intervals during the marker. For each input sample, the detector has to decide whether the gap was present or not. This is a standard signal detection problem.

With standard deviation in spike jitter σ_s=0.1 ms (assumed to be identical for spikes marking the gap, and spikes marking other inter-pulse intervals), and using d'=1 for 76% correct decisions, μ_2 is calculated as 1.14 ms. The gap threshold is then μ_2 - μ_1. Hence, the shortest detectable gap is 0.14 ms for this example. More generally,

$$d' = \frac{gap\ threshold}{\sqrt{\sigma_{s_1}^2 + \sigma_{s_2}^2}} = \frac{gap\ threshold}{\sqrt{2}\sigma_s} \tag{4.10}$$

if σ_{s1}=σ_{s2}, which is assumed to be true. Hence for d'=1 the gap threshold is given by

$$gap\ threshold = \sqrt{2}\,\sigma_s \tag{4.11}$$

for the case of 100% entrainment.

2.3.2 Gap detection based on multiple fibres when entrainment is less than 100%

More generally, the detector will observe M parallel neural channels (M adjacent or closely spaced nerve fibres), of which not all spike trains will be 100% entrained. A stimulus on a particular electrode pair will produce a current distribution with current decaying away from the electrode, so that it may be expected that some fibres close to the electrode will have 100% entrainment, but distant fibres may not fire at all, and some fibres will have intermediate entrainment. Fibres stimulated considerably above their thresholds will have 100% entrainment, but fibres stimulated near threshold will not have a spike probability of one on each stimulus pulse.

2.3.2.1 Model assumptions

Several assumptions are made for modelling purposes. These assumptions are intended to fulfil one of two purposes: either they reflect a certain belief about the nature of the gap detection mechanism, or they are meant to disregard "noise" so as to focus on the underlying signal processing hypothesized to take place.

(1) It is assumed that the central detector observes an attentional window of nerve fibres situated midway between the two markers when the markers are not presented on the same electrode pair. This observation window is chosen to provide optimal detection probability. If the observation window is closer to one electrode than to the other, one electrode might elicit high spike entrainment, while the other electrode does not elicit any neural response in the observation window. The gap will then not be detected. An observation window midway between the two marker electrode positions will provide optimal detection probability.

(2) It is assumed that this observation window cannot be of any given spatial extent, but is limited. In the current model, the observation window is assumed to be limited to one critical band or auditory filter. The observation window is essentially just an off-frequency auditory filter. The psychophysical concepts of critical bands, auditory filters and off-frequency listening are discussed in (Patterson and Moore, 1986).

(3) Finally, it is assumed that the observation window can shift along the axis of the cochlea with a resolution of one nerve fibre, i.e. the M nerve fibres observed can be shifted by one nerve fibre towards the apex or base. This seems to be a reasonable assumption, as critical bands shift dynamically to centre on a given stimulus frequency (Patterson and Moore, 1986).

2.3.2.2 Inter-spike interval probability density function for less than 100% entrainment

The further the marker electrode pairs are apart, the more distant the observation window will be from the electrodes, and the smaller the probability of 100% entrainment becomes. The inter-spike interval histogram (ISI histogram) measured on a single fibre has more than one

mode if entrainment is less than 100%. These modes occur at multiples of the stimulation pulse repetition period. The standard deviation of each mode is σ_s. If the ISI histogram is normalized to an area of 1, it is the pdf (probability density function) of the inter-spike interval of a single fibre (referred to as the ISI pdf in the text that follows). A typical ISI histogram is shown in figure 4.3.

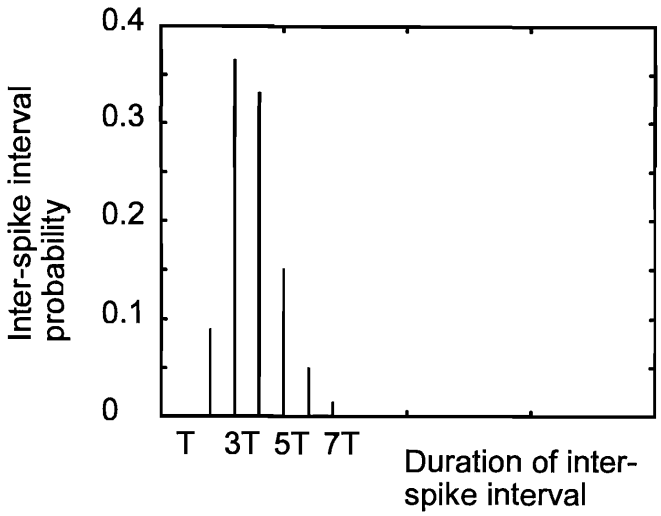

Figure 4.3

A typical ISI pdf for entrainment less than 100%. T is the stimulation pulse repetition period. This figure was calculated using the model of (Bruce et al., 2000). Note that although the figure shows a mode standard deviation of σ_s=0, mode standard deviation is typically up to 0.1 ms. The model used here does not take mode standard deviation (spike jitter) into account.

Assume now that the task is to detect the gap when there is not 100% entrainment. The signal detection task of the central detector is now complicated by the multi-mode pdfs that characterise the two conditions that have to be discriminated, i.e. the pdf of inter-spike intervals when a marker is observed, and the pdf of inter-spike intervals when the gap occurs. The first two modes in these two pdfs will be at T and T+gap respectively, as shown in figure 4.4. It is clear that, to achieve a large fraction of correct decisions, T+gap will be more

distant from T than in the single-mode pdf case. Hence, in this case the gap threshold will be determined by the standard deviation of the multi-mode pdf and not by the spike position jitter.

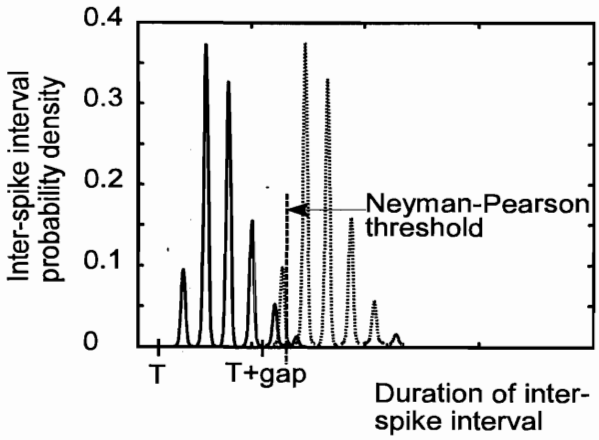

Figure 4.4

Two ISI pdfs, with first mode (of zero amplitude) at T and T+gap respectively, with T+gap chosen for high gap detection probability in this figure.

The model of Bruce, as described in Bruce et al. (2000), Bruce et al. (1999a), Bruce et al. (1999b) and Bruce (1997) calculates the probability of a spike occurring on each stimulation pulse in a pulse train for a given current distribution and stimulation pulse repetition frequency. The complete mathematical model is derived in Bruce et al. (2000) and the derivation is not repeated here. Their model implementation in Matlab is employed for some of the calculations in the current model (with permission from the author of the code).

The Bruce model calculates the normalized ISI histogram internally. It does not take spike position jitter into account. Typical ISI histograms obtained with the Bruce model are shown in figure 4.5.

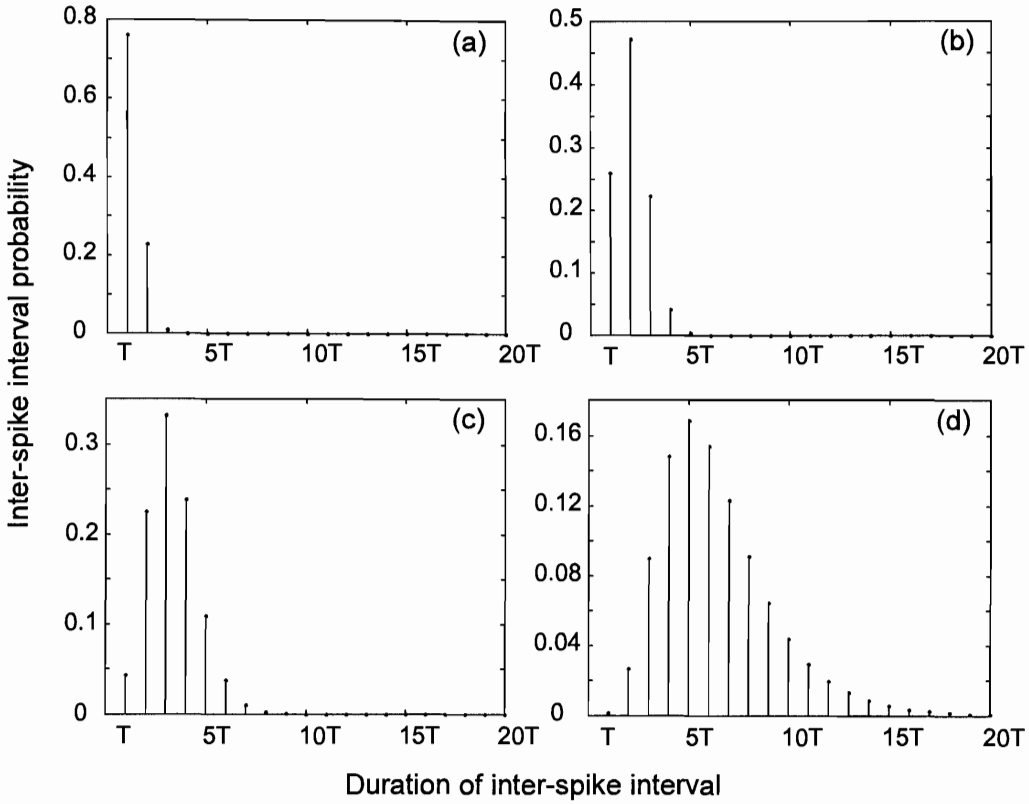

Figure 4.5

ISI pdfs (with no jitter) for several situations in which entrainment is not 100%. The probability of a spike occurring on each stimulus pulse is as follows: (a) P(spike)=0.8, (b) P(spike)=0.5, (c) P(spike)=0.3 and (d) P(spike)=0.16.

Bruce uses the concept of renewal time in his model. The renewal time is the waiting time between the occurrence of one spike and the next. The average renewal time and standard deviation in renewal time are calculated by the Bruce model. These are respectively the mean and standard deviation of the ISI pdf. For example, the average renewal time in figure 4.5a is 1.25T and the standard deviation in renewal time is 0.46T, where T=1 ms is the period of the stimulus pulse train. The average renewal time in figure 4.5c is 3.3T and the standard deviation in renewal time is 1.25T.

2.3.2.3 Approximation to the ISI pdf

To simplify calculations, the ISI pdfs are approximated by their envelopes. For small standard deviation in renewal time, the envelope of the ISI pdf is well approximated by a gamma pdf,

$$pdf(x) = \frac{a^{b}\, x^{b-1}\, e^{-ax}}{\Gamma(b)}, \tag{4.12}$$

where x is the time axis, and a and b are parameters used to fit the gamma pdf to the ISI pdf envelope. Parameters a and b together determine the mean and standard deviation of the gamma pdf. Parameter b determines the order of the gamma function. To obtain a good fit to the ISI pdf data, it was found that a can be taken as

$$a = \frac{2}{\sigma_r}, \tag{4.13}$$

where σ_r is the standard deviation in renewal time calculated by the Bruce model. For small σ_r (below 2 ms), the fit is quite good for a gamma function of order b=5. For larger σ_r, smaller values of b are required to obtain a good fit. A polynomial was fit to the required b values for values of σ_r between 2 ms and 100 ms

$$b(\sigma_r) = p_1\sigma_r^7 + p_2\sigma_r^6 + p_3\sigma_r^5 + p_4\sigma_r^4 + p_5\sigma_r^3 + p_6\sigma_r^2 + p_7\sigma_r + p_8\,. \tag{4.14}$$

The polynomial coefficients are given in Appendix 4.A.

2.3.2.4 Combining information from M channels

Assume now that the observation window is M neural channels wide (i.e. M nerve fibres terminate on the central detector). The information from the M channels is assumed to be combined optimally. The ISI pdfs for the M channels in the observation window are very similar if the observation window is not wider than one critical band, and may be approximated by an observation of M identical neural channels. For M identical channels, d'_M improves with the square root of M,

$$d_m = \sqrt{M}\, d', \tag{4.15}$$

where d' is for each individual channel (Green and Swets, 1966).

2.3.2.5 Calculation of the gap threshold

The gap threshold is now obtained as follows. First, the d' required in each individual channel is calculated from equation 4.15, assuming that the gap threshold is reached when $d'_M=1$. This is an equivalent d', as d' is only defined for Gaussian pdfs. From this d', the required probability of detection P_d in each channel is calculated, for a 2IFC experimental context.

$$P_d = 1 - Erfc\left(\frac{\sqrt{2}\ d'}{2}\right). \tag{4.16}$$

P_d is

$$P_d = \int_{x_{th}}^{\infty} pdf(x|T + gap)\,dx\,. \tag{4.17}$$

The pdf in this equation is the inter-spike interval pdf, conditioned on the occurrence of the gap. The integral is from x_{th}, the detection threshold that the detector uses. This detection threshold is obtained by the Neyman-Pearson criterion (Kay, 1998), which employs a constant false alarm probability P_{fa}. A false alarm probability of $P_{fa}=0.05$ is used, and x_{th} is calculated from

$$P_{fa} = \int_{x_{th}}^{\infty} pdf(x|T)\ dx\,. \tag{4.18}$$

Equation 4.17 must then be solved for T+gap. The integrals in equations 4.17 and 4.18 can be found in closed form. The solution to the integral

$$\int_{x_0}^{\infty} \frac{a^b x^{b-1} e^{-ax}}{\Gamma(b)}\ dx \tag{4.19}$$

is

$$\frac{\Gamma(b, x_0 \cdot a)}{\Gamma(b)} . \tag{4.20}$$

The definitions of the gamma function $\Gamma(b)$ and incomplete gamma function $\Gamma(b,a)$ are given in Appendix 4.A.

Equations 4.17 and 4.18 are nonlinear equations that can be solved with optimization procedures. The gap threshold model was implemented in Matlab. In the Matlab implementation, equation 4.18 is first solved for x_{th}, using the *fsolve* function in the Matlab Optimization Toolbox. This routine employs a Newton method nonlinear least squares algorithm to solve (a system of) nonlinear equations.

With x_{th} known, and the required P_d known from equation 4.16, the gap threshold is obtained from equation 4.17. In implementation it is equivalent, but easier, to solve for the value of x_1 (using the fsolve function) that satisfies

$$\int_{x_1}^{\infty} pdf(x|T)\, dx = P_d . \tag{4.21}$$

The gap threshold is then

$$x_{th} - x_1 . \tag{4.22}$$

2.3.2.6 Software implementation

The procedure defined by equations 4.12 to 4.22 was used to calculate the gap threshold for electrical stimulation when entrainment of some nerve fibres in the observation window was less than 100%. The gap threshold was calculated from equation 4.11 for 100% entrainment. All calculations were done in Matlab 5.3 on a Pentium III based computer running Windows 2000.

2.4 Model parameters

The following model parameters can be varied: neural parameters of fibre threshold and RS (relative spread, a parameter that characterizes the slope of the rate-intensity function, Bruce et al., 2000), current distribution, distance between electrode and fibres, extent of the observation window, and stimulation parameters (intensity, pulse width and pulse repetition frequency). It is shown that with realistic choices of model parameters, predicting measured gap thresholds is possible.

2.4.1 Current distribution

A simple exponential model of current decay, which assumes a homogeneous resistive medium, was one of the two models of current spread investigated in the current study. Bruce et al. (1999b) approximated the current distribution with a point source of current at the active electrode, with a current decay of 4 dB/mm for bipolar stimulation. The model and measurements of Kral et al. (1998) found a current decay of between 4 and 8 dB/mm for bipolar electrical stimulation with the Nucleus-22 electrode array. Electrodes were spaced 0.75 mm apart. Black et al. (1983) measured current decay of 6 dB/mm close to the bipolar electrode (within 1 mm of the electrode), but slower current decay further away from the electrode. Various rates of decay were investigated as appropriate models for the data.

The three-dimensional spiralling finite element model of Hanekom (2001) does not assume a homogeneous medium, but attempts to model the impedance characteristics of the different types of tissue in the cochlea more accurately. Her model uses various electrode positions to predict the voltage distribution in the cochlea. The voltage distribution on the cochlear nerve is then used as input to a nerve fibre model that predicts which fibres will fire. The model clearly shows that, for bipolar stimulation, two peaks of neural activity exist close to the active and return electrodes. The peaks do not occur simultaneously, but on each phase of the biphasic stimulation pulse. The model does not take refractory effects into account.

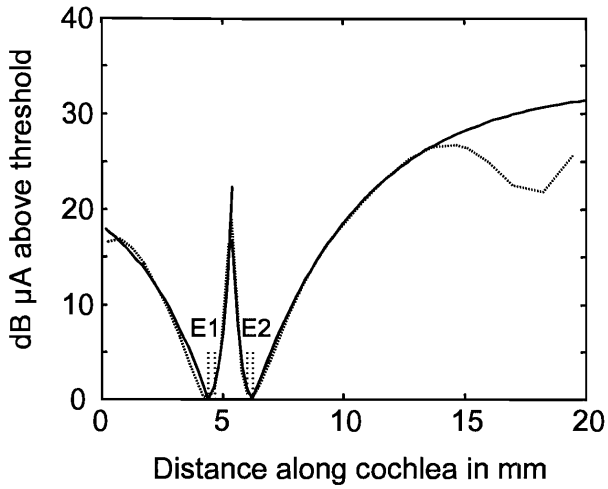

Figure 4.6

The figure shows predicted neural thresholds obtained by the finite element model of Hanekom (2001) (dotted line) along with a curve fit to these data (solid line). The dashed lines E1 and E2 on the figure mark the positions of the two electrodes in a bipolar pair (BP+1 stimulation mode).

Hanekom's results are given as threshold predictions. The threshold of the nerve fibre that fires at the lowest stimulation current (typically a fibre closest to an electrode) is used as reference, and the thresholds of fibres further away from the electrodes are calculated relative to this reference threshold. An example is shown in figure 4.6. For use in calculations, curves have been fit (figure 4.6) to the model-predicted data of Hanekom (2001). Hence, the threshold current (stimulation current at the electrode) of each nerve in the observation window can be calculated.

Assuming that fibres have fixed thresholds, it can be calculated how far above threshold a fibre is stimulated,

$$I_a = I_e - I_{e,th}\,, \tag{4.23}$$

where I_a is the current relative to threshold (in dB µA), I_e is the electrode stimulation current

and $I_{e,th}$ is the electrode current at which the fibre reaches threshold. Then the current at position x is given by

$$I_x = I_{th} + I_a \,, \tag{4.24}$$

where I_{th} is the fixed fibre threshold. The I_x values for all positions x in the observation window define the current spread profile in this window. Position x is defined as the linear distance along the axis of the cochlea, as shown in figure 4.7. Figure 4.7 shows how the physical setup is modelled in the current model. The distance y in this figure is the shortest distance between the electrode array and the neural plane, while the distance z is the direct distance between a specific electrode and a specific nerve fibre.

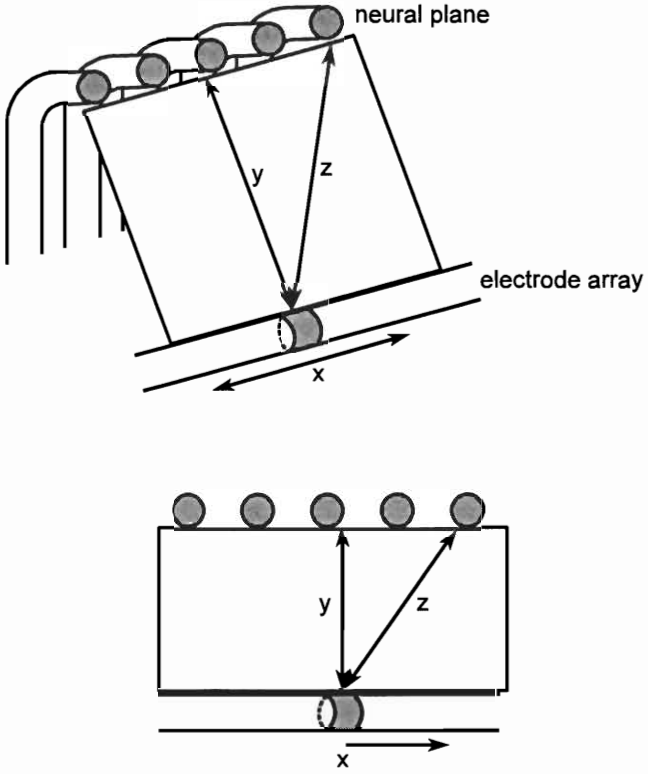

Figure 4.7

This figure defines the spatial relationship between the electrode array and the closest point of stimulation on the neural plane.

The current distribution model in equation 4.24 was the second of the two models of current spread investigated in the current study.

2.4.2 Distance between electrodes and nerve fibres

Distance y in figure 4.7 is the shortest distance between the electrode array and the neural plane. In the Bruce model (Bruce et al., 2000), y=0. More realistically, the electrode array is further away from the neural plane in the base region of the cochlea and nearer to the neural plane in the apex region as a result of the tapering of the cochlea (figure 4.8). Typical values are y=0.8 mm 25 mm from the base, and y=1 mm near to the base of the cochlea (Shepherd et al., 1993). In the Hanekom (2001) model, the electrode is 0.62 mm from the neural plane for an electrode that lies against the outer wall of the cochlea.

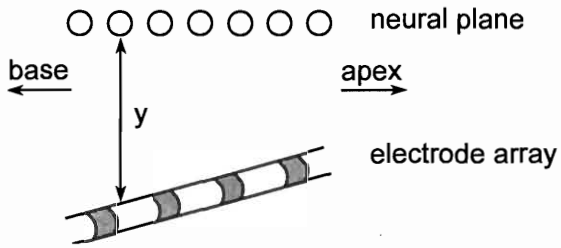

Figure 4.8

The electrode array is closer to the neural plane towards the apex. The distance y varies linearly along the length of the cochlea.

In the current model, fixed distance between the electrode array and neural plane, and also varying distance, were investigated. The fixed distance was taken as 0.5 mm and the electrode array that varied in distance from the neural plane was 0.1 mm away at the apex and 2 mm at the base. Although these values were not realistic, they were chosen to amplify the effect of electrode distance. It turns out that electrode distance has little influence in the model.

2.4.3 Rate-intensity function of nerve fibres

Electrically stimulated nerve fibres have very limited dynamic range, and this is also a function of the state of the nerve fibres. The dynamic range of input intensity (between threshold and saturation) can be as little as 2 dB μA for fibres in a non-deafened cat (Javel and Shepherd, 2000). For the non-deafened cat as well as for a short-term deaf animal, the rate-intensity function is logarithmic (Javel and Shepherd, 2000). However, for the long-term deaf animal, wider dynamic ranges are found, and the rate-intensity function is linear. For the current model, which is intended to model psychoacoustic data of subjects that have been deaf for a long time, it is assumed that the fibre rate-intensity function follows the pattern seen in long-term deaf animals.

The saturation discharge rate, and consequently the dynamic range, is also determined by the stimulation pulse rate for electrical stimulation. Spike rates can be entrained to pulse rate up to very high pulse rates (800-1000 Hz), although some fibres reach saturation rates at lower pulse rates (Javel, 1990; Javel and Shepherd, 2000), especially in long-term deaf ears.

Bruce et al. (1999b) determined mean values and standard deviations for fibre thresholds and RS for the population of (non-deaf) nerve fibres measured by Dynes (1996) (see also Dynes and Delgutte, 1992) and modelled by Bruce. The average fibre threshold was 46 dB μA and the average RS was 0.14. However, as is shown in figure 4.9, larger values of RS replicate the rate-intensity data much better. In the current model, fixed neural parameters (for threshold and RS) are assumed, and specifically, the data for neuron 3-21 as documented in Bruce et al. (1999b) is used. Neuron 3-21 had RS=0.151. In the current model, the effect of RS=0.151, RS=0.3 and RS=0.5 are investigated.

2.4.4 Other stimulation parameters

The following stimulation parameters were fixed in the current model.

The observation window was never wider than one critical band. The number of hair cells per critical band is around 150 (Zwicker and Fastl, 1990), and it was assumed that the central

detector used information from anything between M=1 and M=150 fibres.

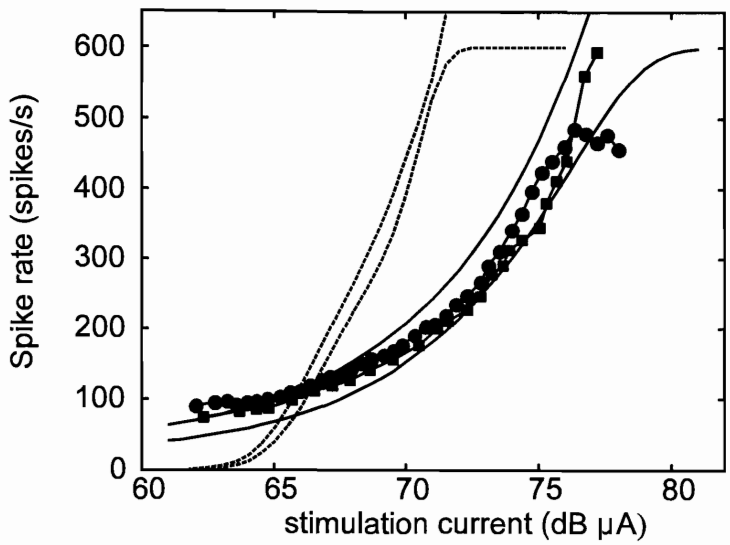

Figure 4.9

The data of Javel and Shepherd (2000) for a long term deaf cat stimulated at 600 pps (●) and at 800 pps (■) are shown together with rate-intensity functions obtained with the Bruce model, with RS=0.5 (solid lines) and RS=0.151 (dotted lines). In both cases, curves for 600 pps and 1000 pps stimulation rates are shown. The 600 pps curves saturate at 600 spikes per second.

Stimulation pulse rate of 1000 Hz and pulse width of 200 μs/phase were used in the model, as these were the parameters used in the psychoacoustic experiments that this model is intended to model. For similar reasons, BP+1 mode was assumed, and it was assumed that the electrode array was the Nucleus-22 design (Clark et al., 1990). Electrodes in a bipolar pair were 1.5 mm apart.

3 RESULTS

3.1 Gap detection tuning curves predicted by model

Figures 4.10 to 4.22 show gap detection tuning curves for various parameter choices in the model. Parameters investigated for their influence on gap detection thresholds are described below.

(1) The effect of the number of fibres in the observation window (M=1 to M=150) was investigated. The width of the observation window was at most one critical band.

(2) The effect of current distribution was investigated. The rate of current decay away from the active electrode site was varied for simple exponential current decay. The twin-peaked current distributions predicted by the model of Hanekom (2001) were also investigated as an alternative current distribution model.

(3) Neural parameters (fibre threshold and RS) were either random (according to the model of Bruce et al., 1999b) or fixed (parameters of neuron 3-21 in Bruce et al., 1999b).

(4) A random component was added to the current distribution to simulate the effects of current decay that varied as a result of a non-homogeneous current path impedance.

(5) The distance between the neural plane and the electrodes was either fixed at 0.5 mm, or varied linearly between 2 mm (near the base) and 0.1 mm (near the apex). These values are not realistic, but were chosen to magnify the effect of the relative distance between the neural plane and the electrodes.

(6) In one embodiment of the model, gap threshold was always calculated from equation 4.17 (which assumes less than 100% entrainment). In a second embodiment, equation 4.11 was used when entrainment was 100%, and equation 4.17 when entrainment was less than 100%. These two conditions are identified as a single process model and dual process model respectively.

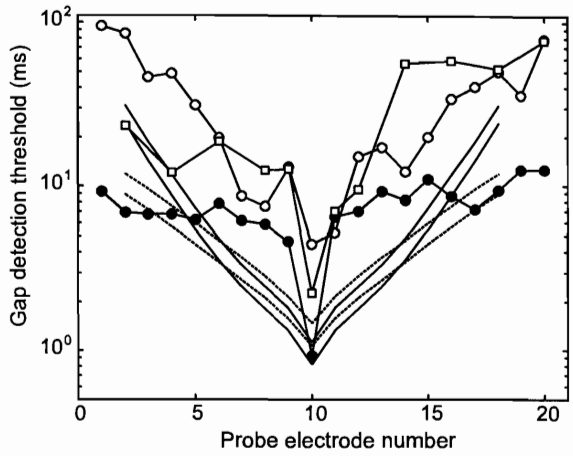

Figure 4.10

Model predictions for gap detection thresholds for a pulsatile stimulus of 55 dB μA. The neural parameter RS was either 0.3 (solid lines) or 0.5 (dashes). In these two sets of curves, either M=1 (upper curve) or M=150 (lower curve). A single process model was employed, and the distance between the electrode plane and neural plane was 0 mm. The exponential current decay was 4 dB/mm. The data with electrode 10 as standard for subjects N3 (○), N4 (●) and N7 (□) are also shown.

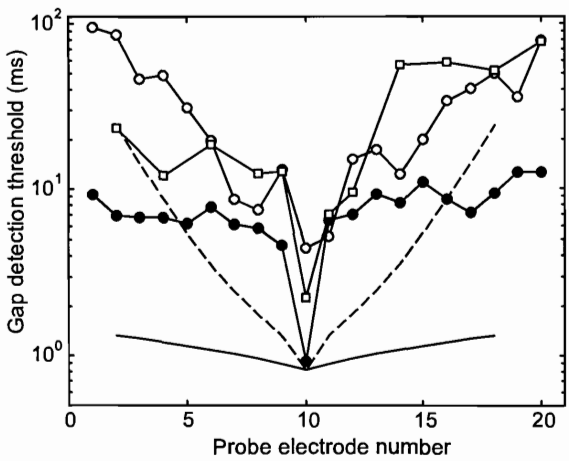

Figure 4.11

This figure shows the effect of a different rate of exponential current decay. The solid curve is for a current decay of 0.5 dB/mm, while the dashed curve is for 4 dB/mm. M=150 in both model curves, RS=0.3, and the subject data are also shown.

Figure 4.10 shows model predictions with M=1 and M=150, for a stimulus of 55 dB μA. A single process model was employed, and the distance between the electrode plane and neural plane was 0 mm. The exponential current decay was 4 dB/mm, and the neural parameter RS was (for a long-term deaf ear) either 0.3 (solid lines) or 0.5 (dashes). The Neyman-Pearson detection threshold was calculated to obtain a false alarm probability of 0.05. The gap detection tuning curves for N3, N4 and N7, with electrode 10 as standard (from Hanekom and

Shannon, 1998, or chapter 2), are also shown. The model-predicted gap tuning curves do not show the sharp tip seen in the data of N4 and N7, but has the shallow bowl shape of the N3 data.

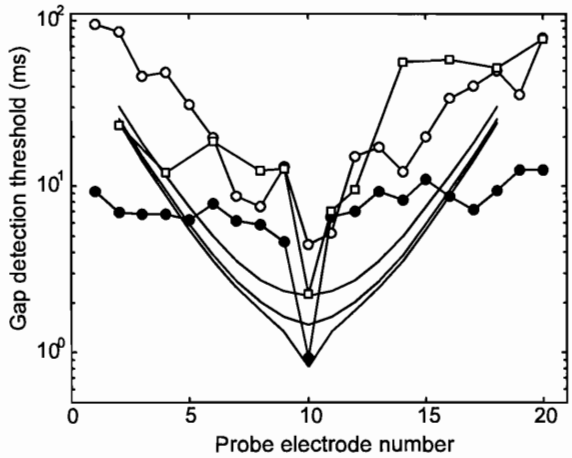

Figure 4.12

This figure shows the effect of the distance between the neural plane and the electrode plane, for a non-varying distance between the electrode array and the neural plane. From top to bottom, the model-predicted curves are for distance y of 1mm, 0.5 mm and 0 mm. Exponential current decay was 4 dB/mm, the stimulus intensity was 55 dB μA, and M=150.

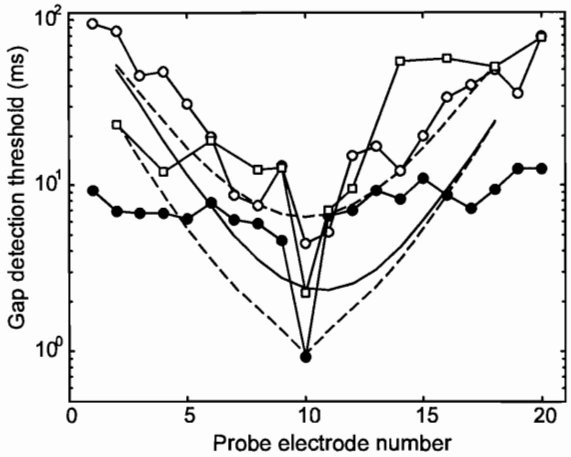

Figure 4.13

The distance between the electrode array and the neural plane varied along the length of the array in this figure (solid curve). The distance varied linearly between 2 mm for the most basal electrode to 0.1 mm for the most apical electrode. This is compared to fixed electrode array distances of 0.1 mm (lower dashed curve) and 1 mm (upper dashed curve).

Figure 4.11 shows the effect of a different rate of exponential current decay. M=150 in both model curves, and the subject data are also shown. The slope of the 0.5 dB/mm model curve is similar to the slope of N4's data, but does not show the sharp tip. A current decay of 4 dB/mm is typical of bipolar stimulation, while 0.5 dB/mm is more typical of monopolar stimulation. The N4 gap detection data exhibit trends that can be predicted by fast current decay (> 8 dB/mm) near the electrode, but to predict trends in the far field, a current decay

more typical of monopolar stimulation is required.

Figure 4.12 shows the effect of the distance between the neural plane and the electrode plane, assuming a non-varying distance between the electrode array and the neural plane. More distant positions for the electrode array result in larger gap detection thresholds, and the sharp tip is not observed for more distant positions.

The distance between the electrode array and the neural plane varied along the length of the array in Figure 4.13. The distance varied linearly between 2 mm for the most basal electrode to 0.1 mm for the most apical electrode. This is compared with fixed electrode array distances of 0.1 mm and 1 mm. The electrode array with linearly varied position is shown to deform the gap tuning curve towards the apex.

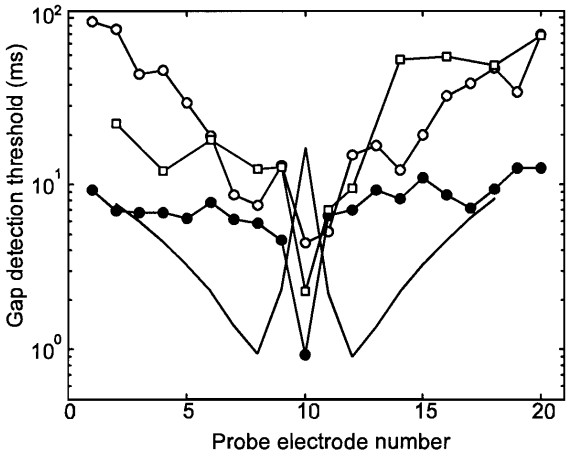

Figure 4.14

Model-predicted gap detection tuning curves when the twin-peaked current distributions predicted by the model of Hanekom (2001) are used. Model parameters are M=150, and Neyman-Pearson threshold=0.1.

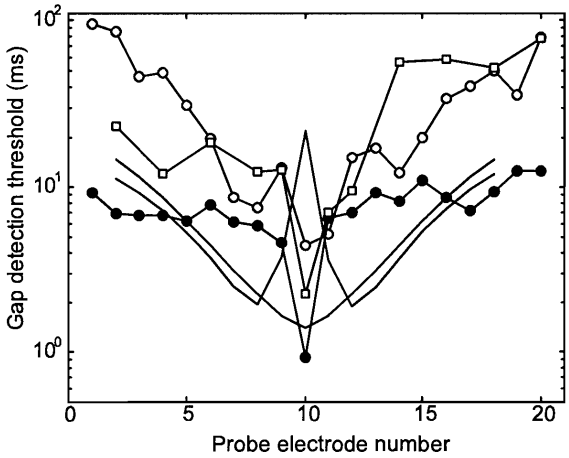

Figure 4.15

The gap tuning curve predicted by the Hanekom current distribution model is compared to a decay of 6 dB/mm.

The twin-peaked current distributions predicted by the model of Hanekom (2001) result in the gap detection tuning curves in figure 4.14. Model parameters are M=150, and Neyman-Pearson threshold=0.1. The twin-peaked current distribution results in a twin-tipped gap detection tuning curve with large gap thresholds when the standard and probe are on the same electrodes. This is not consistent with the trends observed in the data. The flanks of the gap tuning curves predicted by the Hanekom model exhibit a 6 dB/mm decay, as shown in figure 4.15 where it is compared to a single-peaked exponential decay of 6 dB/mm.

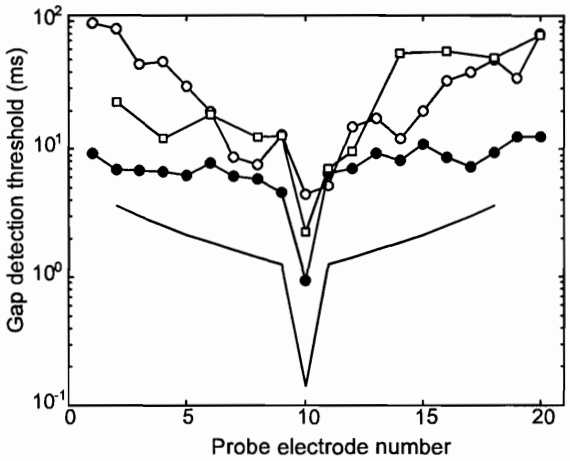

Figure 4.16

The dual process model predicts the sharp tip at high intensity (57 dB μA).

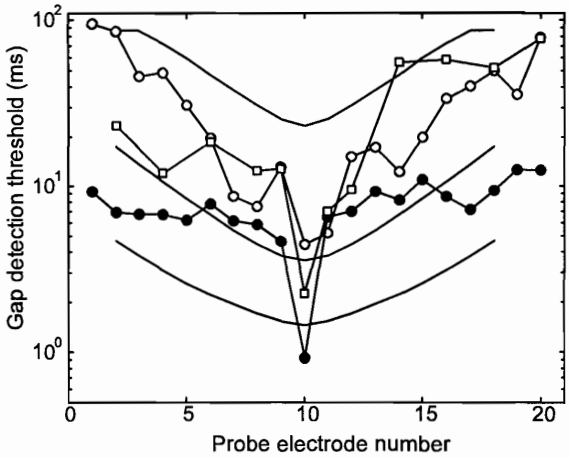

Figure 4.17

The effect of neural threshold is shown at fixed stimulation intensity of 50 dB μA, with M=1 and RS=0.3. From top to bottom, the neural threshold was 55 dB μA, 49 dB μA and 45 dB μA.

The dual process model predicts the sharp tip at high intensity (figure 4.16). A 2 dB/mm decay is used to obtain the simulation results in figures 4.16 and 4.17. This current distribution produced tuning curve flanks consistent with the data of N7. The dual process model is employed in figure 4.17 and M=1. The effect of neural threshold is shown at fixed stimulation intensity of 50 dB μA. As neural threshold increases, the gap threshold also increases, as expected.

With a 2 dB/mm current decay, different values of stimulation intensity result in gap tuning curves that show some of the trends observed in the data (figure 4.18). At lower intensities, the model predicts a bowl-shaped curve similar to the data of N3. At higher intensities, the model predicts the sharp tip seen in the data of N4 and N7.

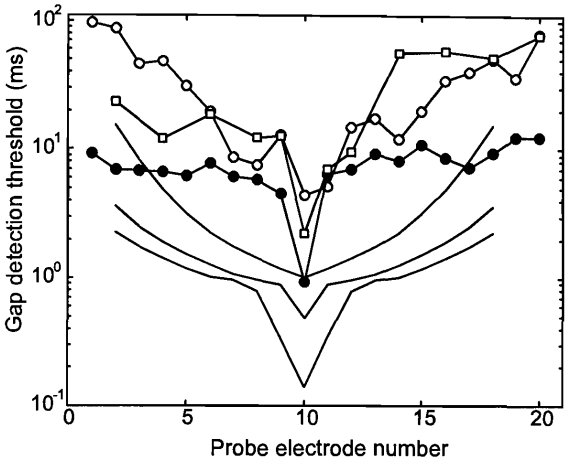

Figure 4.18

The effect of intensity of stimulation on predicted gap thresholds. From top to bottom, stimulus current was 53 dB μA, 55 dB μA and 57 dB μA. Other parameters are y=0, RS=0.151, current decay is 2 dB/mm, M=1.

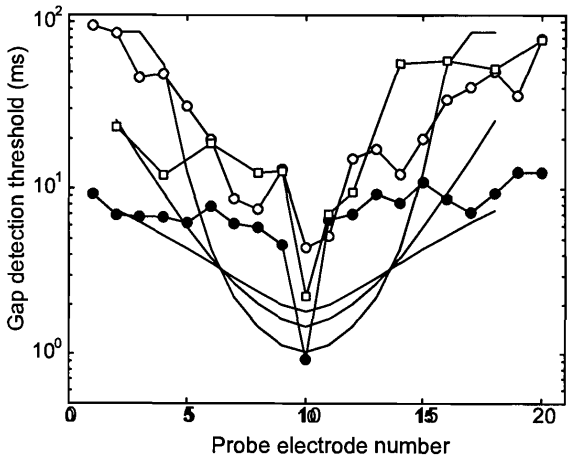

Figure 4.19

The influence of neural parameter RS (relative spread) is shown in this figure. The shallow curve is for RS=0.6, the steepest curve is for RS=0.15, and the third curve is for RS=0.3. Other parameters are M=150, stimulation intensity is 55 dB μA, and current decay is 4 dB/mm.

A likely explanation is that the electrode array for N3 is more distant from the neural plane than that of N4. The argument is that the gap tuning curves for N3 and N4 where obtained at similar loudness levels. Possibly then, the N3 gap tuning curve may also have shown the sharp tip at higher intensities. This in turn suggests that the current distribution for N3 is wider, although figure 4.11 suggests a wider (far field) current distribution for N4 (or slower far field current decay). However, it is also seen that the slopes on the flanks of the gap tuning curves are shallower at higher stimulation intensities, similar to the trend in N4's data, which supports the idea that N4's array is closer to the nerve fibres.

The neural parameter RS (relative spread) influences the fibre rate-intensity curve and therefore affects the shape of the gap tuning curve (figure 4.19). When RS is larger, the tip of the gap tuning curve is sharper, and the slopes on the flanks of the curves are steeper.

When the neural parameters are allowed to be random (in accordance with Bruce et al., 1999b), the gap tuning curves show the jagged trends seen in the data. When the neural threshold is allowed to vary over a 10 dB range, large variance is seen in the gap tuning curves (figure 4.20), while a range of 1 dB or 5 dB simulates the trends in the data more closely (figure 4.21).

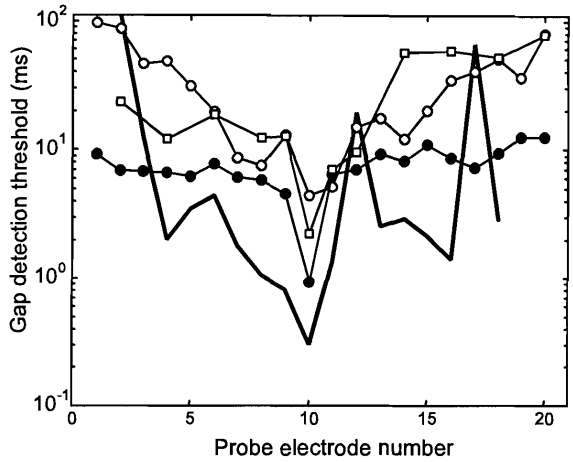

Figure 4.20

The neural threshold varies over a 10 dB range. Other parameters are M=150, stimulation intensity is 50 dB μA, and current decay is 4 dB/mm.

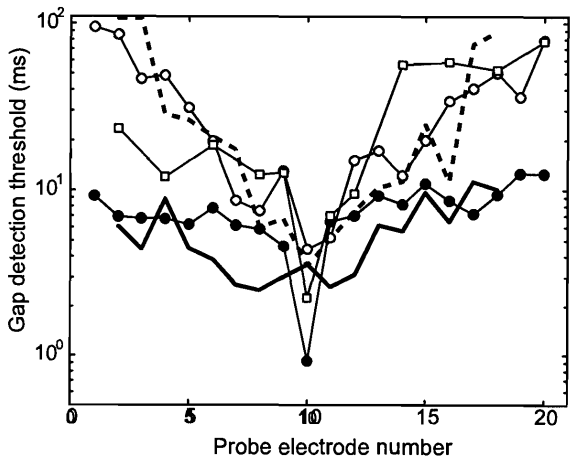

Figure 4.21

The neural threshold varies over a 5 dB range in this figure. Other parameters are M=150, stimulation intensity is 50 dB μA, and current decay is 1 dB/mm (solid line) or 4 dB/mm (dashed line).

Using fixed neural parameters, but adding a random component of standard deviation of just 1 dB to the current distribution, it is seen in figure 4.22 that the non-monotonicity of the data can also be predicted by variation in current decay. The figure shows that the trends of data of N3 are predicted (solid line) by a general trend of 4 dB/mm current decay, with a 1 dB standard deviation in the current that reaches the (fixed threshold) fibres. Non-monotonic

current decay can result from non-homogeneous impedance paths. The general trends of N4's data are predicted (dashed line) by current decay of 1 dB/mm (with a 1 dB standard deviation in the current).

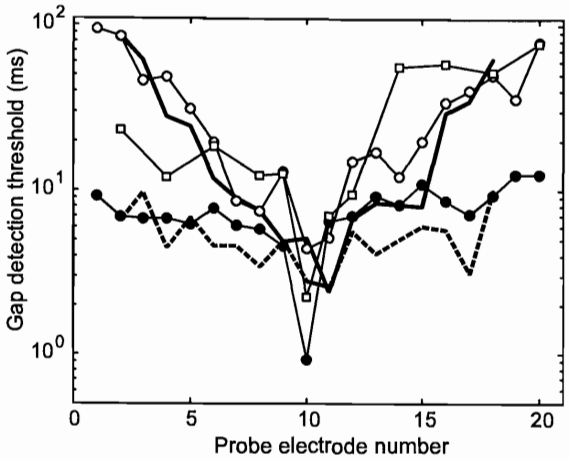

Figure 4.22

A random component of standard deviation of 1 dB is added to the exponential decay current distribution. The solid line has a 4 dB/mm exponential current decay, and the dashed has a current decay of 1 dB/mm.

3.2 Current distributions predicted by model

Figures 4.23 to 4.25 show the electrode current required by the model to obtain the measured gap tuning curves for the three subjects. These curves assumed an electrode-neural distance that varied across the length of the electrode array. A general trend in these curves is that larger currents are required to obtain the measured gap detection thresholds when the electrode is more distant from the nerve fibres. However, the curves are non-monotonic and all three curves have a peak at the standard electrode, so that larger currents are required to obtain the small values of gap threshold that are generally observed when both markers are on the same electrode.

From these curves, the current distribution is calculated (figures 4.26 to 4.28), i.e. for a fixed

electrode stimulation current, these curves show the calculated current at a number of positions on the neural plane. More specifically, the model can only calculate the currents at the set of positions of observation windows used by the model.

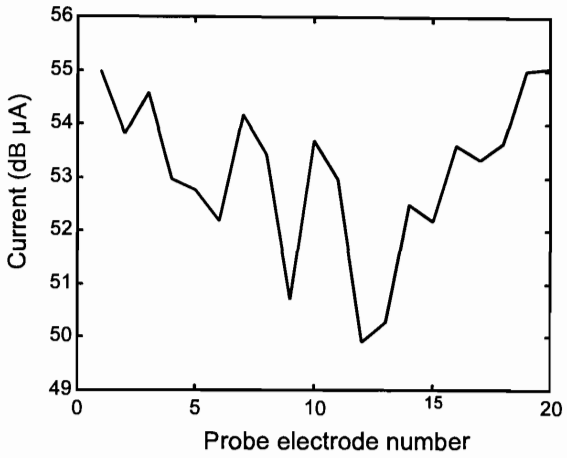

Figure 4.23

This figure shows the electrode current that is required in the model to obtain the measured (Hanekom and Shannon, 1998) gap tuning curves for subject N3. Model parameters are as follows. M=1 and RS=0.3, while the model assumed a 4 dB/mm current decay.

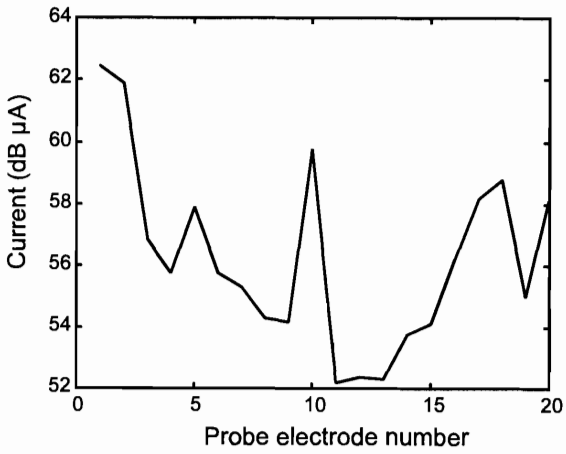

Figure 4.24

Same as figure 4.23, but for subject N4.

The current distribution curves obtained depend on model assumptions. In figures 4.26 to 4.28, an electrode array with varying distance y to the neural plane was assumed. RS=0.3 was used in these simulations. A numerical value for the current decay model parameter (e.g. 4 dB/mm) is required by the model to calculate the gap thresholds in the optimization routine that solves for the required current. Different choices of this parameter lead to slightly different predictions for the current distribution. In calculation of the current spread, the current decay parameter will specify only the general trends in the data. As the results show, the actual (model-calculated) rate of decay is non-monotonic and not necessarily close to 4 dB/mm. This is as a result of variations in current pathways and non-homogeneous impedance.

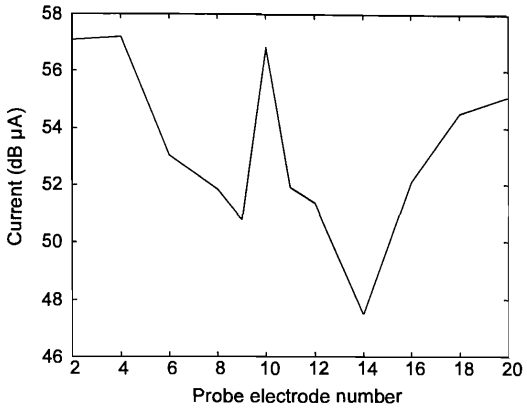

Figure 4.25

Same as figure 4.23, but for subject N7.

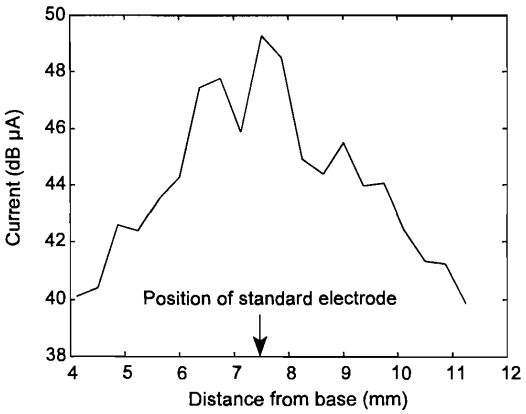

Figure 4.26

The current distribution curve for N3 as calculated from figure 4.23, assuming an electrode array with varying distance y to the neural plane.

Figure 4.26 shows a wide, unfocussed current distribution for N3, with a rate of current decay of 2.7 dB/mm (towards base) and 2.5 dB/mm (towards apex). N4 has a sharp current peak at fibres closest to the standard electrode position and then a gradual decay of current towards the more distant nerve fibres (< 1 dB/mm). Hence, N4 has sharply focussed stimulation close to the electrode, but also a wide activation pattern with higher levels of current than N3 and N7 still present far from the electrode (figure 4.29).

N7 also has a sharply focussed current distribution close to the electrode (8 dB/mm towards the apex), and a somewhat more gradual decay in current of 3.2 dB/mm (towards the apex) and 2.67 dB/mm (towards the base) when measured from the tip to the tail on either side of the tip.

The current intensity does not decay more than 14 dB for any of the subjects even at the most distant nerve fibres modelled. Predictions are not available throughout for the current at the –10 dB point, as the current has not always decayed that much. As a measure of the focussing of current, the –6 dB focussing width and the –10 dB focussing width are calculated. Curves

were extrapolated if the current did not decay by 10 dB or more to obtain the values for focussing width. The –6 dB focussing widths for the subjects are 4.4 mm (N3), 0.7 mm (N4) and 1.1 mm (N7). The –10 dB focussing widths for the subjects are 8 mm (N3), 5.3 mm (N4) and 5.3 mm (N7).

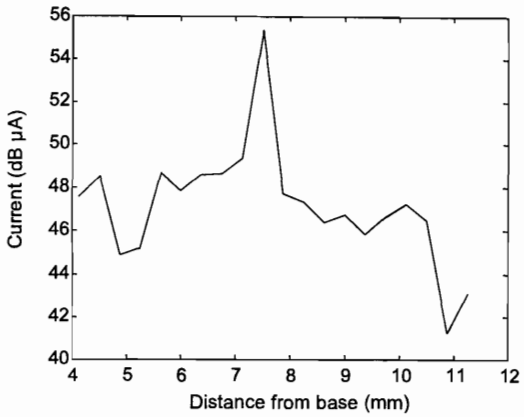

Figure 4.27

Same as figure 4.26, but for subject N4 and calculated from figure 4.24.

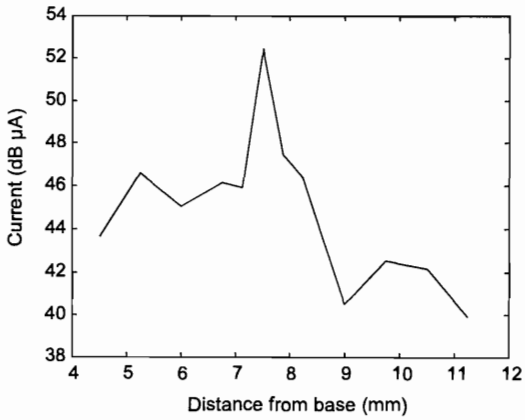

Figure 4.28

Same as figure 4.26, but for subject N7 and calculated from figure 4.25.

With different model assumptions than those for figures 4.26 to 4.28, different model-calculated current distribution curves are obtained. The predicted current distribution does not change by more than 5% when the electrode array is at fixed distance of 0.5 mm from the neural plane, while the trends remain the same. However, when the model assumption for the current decay rate is different, the predicted current distributions are notably different to those obtained in figures 4.26 to 4.28. A current decay of 4 dB/mm appears to model the gap data for N3 quite well (figure 4.22), but N4 has a current decay of closer to 1 dB/mm on the flanks (figure 4.22), while the N7 data is probably modelled better by a 1 dB/mm decay on the base flank and a 4 dB/mm decay on the apex flank of the data. Using 1 dB/mm for both the N4 and N7 data, the current distribution curves in figure 4.30 and 4.31 are obtained.

Particularly notable in these model-calculated current distribution curves are the widely varying patterns of predicted current distribution in these three subjects. Many psychophysical studies

have reported considerable inter-subject variability and this is regarded as a major obstacle in the way of progress in development of more advanced cochlear implants.

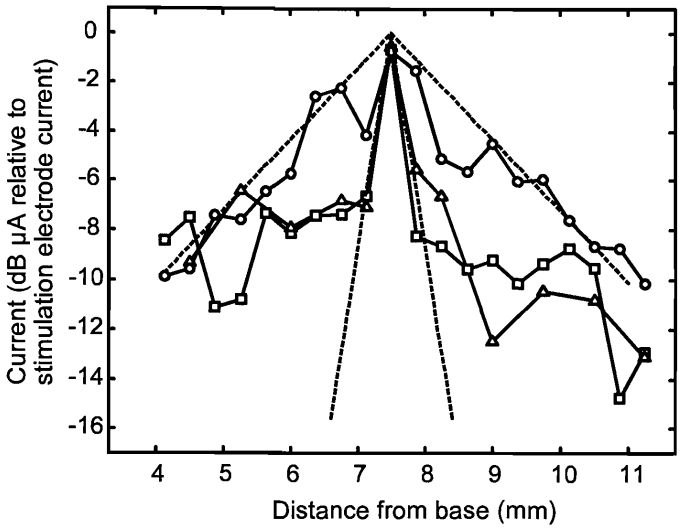

Figure 4.29

Current distributions for all three subjects plotted on the same graph (circles: N3; squares: N4; triangles: N7). Current decay is plotted relative to the current that reached the fibres closest to the standard electrode. Also shown (dashed lines) are two exponential current decay curves with length constants of 0.5 mm and 3 mm respectively (decay of 8.7 dB/mm and 1.4 dB/mm respectively).

Published data for *current* distributions in cochlear electrical stimulation are scarce. More often, *voltage* distributions are measured (Ifukube and White, 1987; Spelman et al., 1995) or modelled (Hanekom, 2001). However, as was shown by Black et al. (1983) and Kral et al. (1998), voltage distributions do not necessarily reflect the current distributions at the neural excitation sites. This is because of non-homogenous impedance in the cochlea. Voltage distributions cause currents and these currents excite nerve fibres. Accordingly, using current distributions to predict which fibres will be excited is more appropriate.

It is noted, however, that some more complex voltage distribution models (Frijns et al., 1995;

Hanekom, 2001) calculate nerve excitation directly from the voltage distributions via finite difference or finite element models that take the non-homogeneous cochlear impedances into account and via Hodgkin-Huxley (or equivalent) nerve fibre models that predict when fibres will fire.

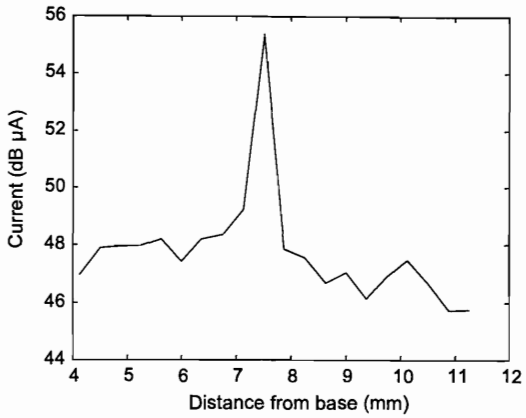

Figure 4.30

With different model assumptions than in figure 4.24, the predicted current distribution for subject N4 is as shown in this figure. The model now assumes a 1 dB/mm current decay.

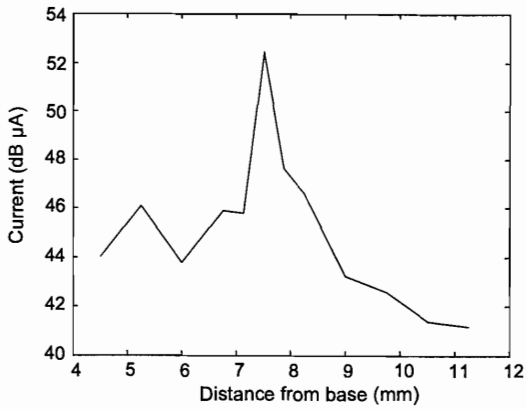

Figure 4.31

Same as figure 4.30, but for subject N7.

As a further note, spatial excitation data are also usually given as threshold data rather than as spatial excitation profiles. Several studies measured the thresholds of fibres at various cochlear positions in response to electrical stimulation at a fixed position in the cochlea (e.g. Van den Honert and Stypulkowski, 1987b; Shepherd and Javel, 1997), but no data on supra-threshold spatial excitation patterns appear to be available.

Figure 4.32 compares the model-calculated current distribution curves to current distribution data from Black et al. (1983). These data were not obtained in vivo, but were measured in a tank model (a 5 mm saline-filled tube). The data show a current decay length constant of 0.7 mm at the tip, which is the same as the length constant obtained by Kral et al. (1998) in their measurements. Close to the peaks the model-calculated current distributions for N4 and N7

follow the data quite well. The tails of the calculated current distributions are elevated by 5-10 dB relative to the tank data.

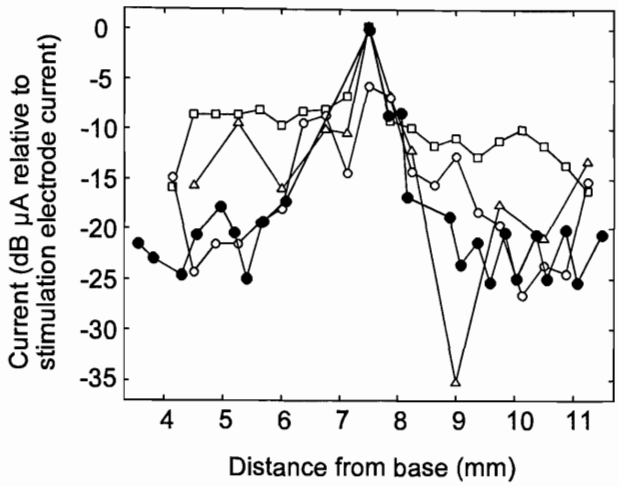

Figure 4.32

This figure compares the model-calculated current distribution curves to measured current distribution data. Filled circles are data from Black et al. (1983). Open symbols are predicted current distributions for the three subjects (open circles: N3; open squares: N4; open triangles: N7).

3.3 Predictions for electrode discrimination from the predicted current distributions

Predictions for current distributions were obtained for all the electrodes for which gap detection tuning curves were available for all three subjects. Predictions were then obtained for the discriminability of electrodes. This was done as follows. The average and standard deviation of each electrode's current distribution was required. As the rate of current decay was different towards the base than towards the apex, the standard deviation was calculated on either side of the peak current. Electrode discriminability was then calculated from

$$d' = \sqrt{\frac{2(m_2 - m_1)^2}{\sigma_{E1}^2 + \sigma_{E2}^2}}, \qquad (4.25)$$

where m_1 and m_2 are the active electrode positions (in mm from the base), and σ_{E1} and σ_{E2} are the standard deviations of the current spread on the appropriate flanks of the current distribution curves of the two electrodes. The predicted electrode discriminability is shown as two-dimensional contour plots (figure 4.33 and 4.35) for N4 and N3 respectively. These figures show how discriminability varies with distance between the electrode pairs. In both cases, a distance of at least two electrodes (in BP+1 mode in the Nucleus cochlear implant, see chapter 2) is required to achieve d' > 1 (defined as the discrimination threshold).

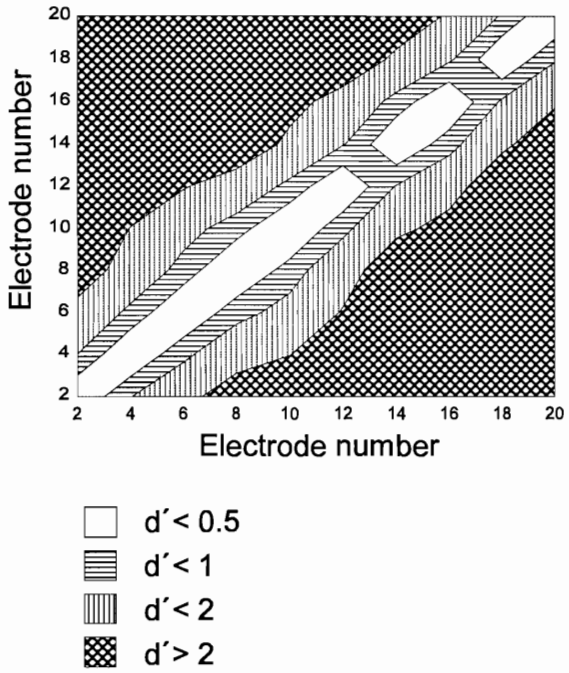

Figure 4.33

Predicted electrode discriminability for N4 in BP+1 mode.

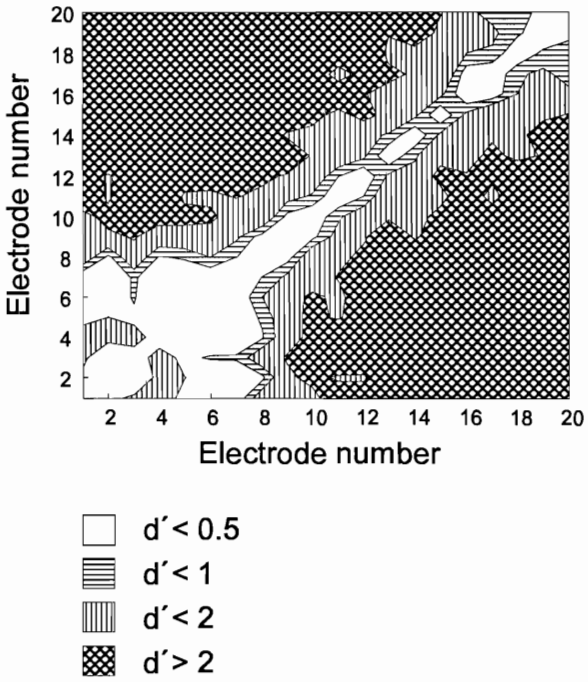

Figure 4.34

Electrode discriminability for N4 (BP+1 mode) measured in a pitch discrimination experiment (Hanekom and Shannon, 1996).

This means that electrodes need to be spaced at least 1.5 mm apart (in the Nucleus cochlear implant, see chapter 2) to be discriminable. As the two electrodes in an electrode pair is 1.5 mm

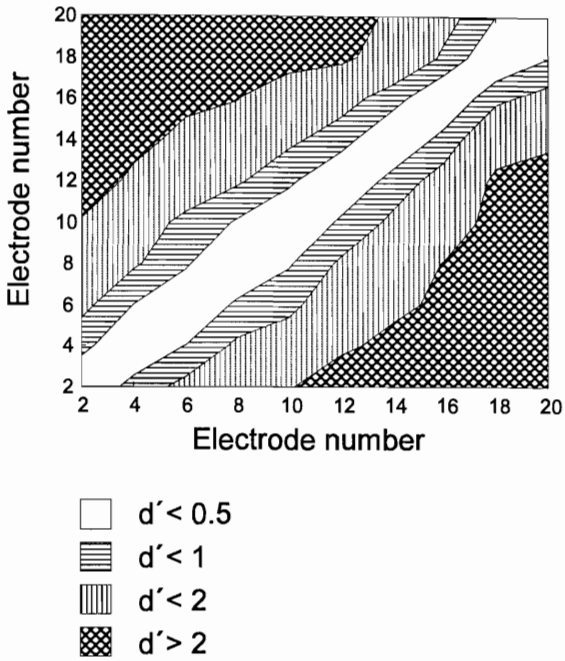

Figure 4.35

Predicted electrode discriminability for N3 in BP+1 mode.

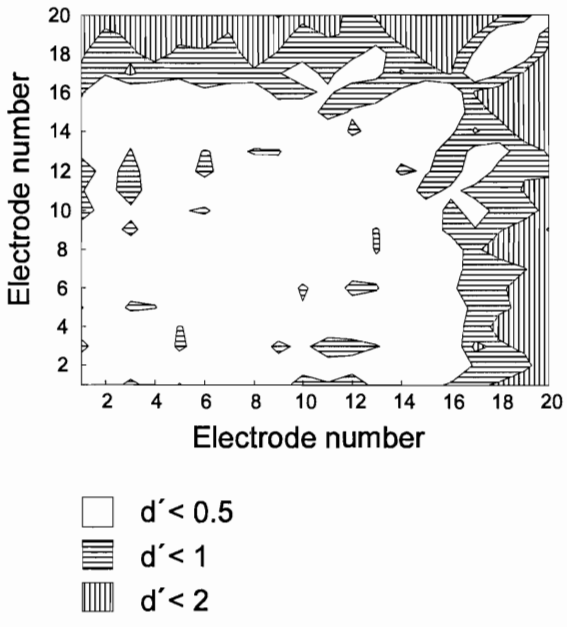

Figure 4.36

Electrode discriminability for N3 (BP+1 mode) measured in a pitch discrimination experiment (Hanekom and Shannon, 1996).

apart, this means that stimuli on overlapping electrode pairs will be poorly discriminated. This is probably because these electrode pairs stimulate the same neural population to a large extent. The predictions in figures 4.33 and 4.35 also suggest that electrodes with closer spacing will be more discriminable for N4 than for N3.

Predicted discriminability of electrodes is compared with electrode discrimination data (figures 3.34 and 4.36) for the same subjects (Hanekom and Shannon, 1996). The predicted discriminability correlates well to the measured electrode discrimination data for N4, but not for N3 or N7 (not shown). The data for N4 suggests that a separation of at least two electrodes

is required to achieve d' > 1, as is also predicted by the model. This suggests that the current distributions predicted by the model is a fair reflection of the actual current distributions for N4.

N3 (and N7, not shown) should have performed better on the electrode discrimination task than what is reflected in the data in figure 4.36 if the current distribution predictions are accurate. Other factors may have played a role in N3's case (and in N7's) in the electrode discrimination task. The actual task was a pitch discrimination task, and it is possible that electrodes were discriminable, but that these subjects were not able to judge pitch. Anecdotaly, N7 reported that he "has always been tone deaf". Thus, the electrode discrimination data do not provide conclusive evidence that the predicted current distributions are correct.

4 DISCUSSION

4.1 Modelling of gap detection data

The model can predict both the magnitude of gap thresholds and the U-shaped curves with the correct choice of parameters. The trends in the slopes on the flanks of the predicted gap thresholds curves follow those seen in the data, and depend primarily on the current distribution and rate of current decay. Realistic choices for rate of decay can predict the slopes.

If an exponential decay is assumed, the model cannot predict the sharp tip seen in the data of N4 and N7, but the shallow bowl is predicted. It is possible that two separate mechanisms exist that determine gap thresholds, so that gap thresholds are very small in the within-channel condition and larger in the across-channel condition. It is possible that a perceptual similarity process plays a role in the across-channel condition as suggested in chapter 2.

However, the model shows that hypothesizing different mechanisms for across-channel and within-channel conditions is not necessary. When entrainment is close to 100%, gap thresholds are determined by the spike position jitter (spike position standard deviation) alone. Gap

thresholds are then expected to be small for pulsatile electrical stimulation, as temporal jitter of spikes is small. This situation is most likely to occur when the two markers are presented on the same electrode.

When entrainment in the observation window is lower that 100%, gap thresholds are primarily determined by the standard deviation of the inter-spike interval pdf and the temporal jitter of spikes does not play an important role. The standard deviation of the inter-spike interval pdf for less than 100% entrainment is typically much larger than temporal jitter, so that gap thresholds are expected to be much larger. Figures 2.5 to 2.7 provides further support for this notion. The sharp tips in the gap detection tuning curves disappear at lower stimulation levels where entrainment should be below 100%. Thus it appears that this model provides a plausible explanation for the origin of the gap detection tuning curves.

Finally, it is not clear why the twin-peaked voltage distribution predicted by Hanekom (2001) fails to be a good predictor for gap thresholds. A less than satisfying explanation is that the nonhomogeneous cochlear impedance introduces enough variability in the current arriving at different fibres to mask the twin-peaked pattern.

4.2 Modelling of current distributions

Predicted current distribution profiles are consistent with tank measurements (Black et al., 1983) of current distribution (figure 4.32) for the first millimeter on either side of the current peaks and the trends are similar throughout the modelled region. Exponential current decay cannot explain the sharp tip, but a more sharply focussed current distribution can explain the sharp tip (see figures 4.26 to 4.28). Differences between model predictions and tank data in the tail sections of the current distributions may be due to differences between the nonhomogeneous cochlear impedances and homogeneous tank impedances. Shepherd and Javel (1997) remarked that current spread may increase in long-term deafness due to demyelination of nerve fibres. The length constant of the predicted current distributions of N4 and N7 is 0.5 mm near the tip, which is comparable to the length constants measured by Kral

et al. (1998). The length constant of the current distribution of N3 is 3 mm, which is also the length constant measured by Black et al. (1983).

Interesting results are presented in figures 4.29 and 4.33. Close to the electrodes, predicted current distributions for N4 and N7 show current decays that are typical of bipolar stimulation, while the current decay of N3 is more reminiscent of monopolar stimulation. The data of N4 and N7 show sharp (predicted) current peaks close to the electrodes, with current decay very similar to what has been obtained in a tank model. The predicted current distribution tails more distant from the electrode follows the trend seen in the tank model data.

The wide current distribution pattern of N3 is reflected in the electrode discriminability data shown in figure 4.36, while the more sharply focussed current distribution (close to the stimulation electrodes) of N4 is reflected in the electrode discriminability data shown in figure 4.34. Even though the tail in the predicted current distribution of N4 is equally far below the current peak than N3's predicted current distribution, N4 has much better electrode discriminability. Thus it appears the tail of the current distribution does not contribute to the listener's ability to discriminate electrodes. This emphasizes the importance of current focussing techniques in stimulus pattern design (Townshend et al., 1987) and electrode designs to obtain better current focussing (Cords et al., 2000).

It is clear from figure 4.36 that N3 had difficulty in discriminating closely spaced electrodes, which may be ascribed to the wide current distribution. Hanekom and Shannon (1996) endeavoured to relate place pitch discrimination data to current spread and the definition of information channels in electric hearing. While the measurement of electrode discrimination relied on the pitch discrimination ability of subjects in the experiments of Hanekom and Shannon, gap detection may provide a more objective approach to arrive at predictions for current distributions. The similarity between the trends seen in the predicted current distributions and the electrode discrimination data is encouraging.

There is, however, still a large discrepancy between the predicted electrode discriminability

pattern and the place pitch discrimination data (figures 4.35 and 4.36). It is possible that the pitch discrimination experiment of Hanekom and Shannon (1996) underestimated the ability of subjects who had poor pitch perception to discriminate electrodes. Experiments that are designed for electrode discrimination (e.g. Collins et al., 1997) rather than for place pitch discrimination would have been more appropriate for comparisons between predictions and data. It is possible that electrode discrimination is better than reflected in the place pitch discrimination data.

As a final remark, predicted current distributions vary widely between subjects, which may be a major factor determining speech recognition ability in cochlear implant users.

4.3 Applicability of the model

The model described in this chapter is only applicable for auditory electrical stimulation, and specifically the situation where the gap is defined as in figure 4.1. If stimulation pulses can occur in the gap, i.e. when the gap is not silent, the model will not necessarily model the task of the central detection mechanism very well. Also, when spikes can occur during the gap (in a model with spontaneous activity), the task changes. These situations were investigated in paragraph 4.2.2. The model is applicable in a gap discrimination situation, but as no gap discrimination data for cochlear electrical stimulation is available, model predictions for the discrimination task were not explored further.

4.4 Free parameters and parameter sensitivity

The model has a small number of free parameters that control different aspects of the gap threshold tuning curves. The U-shaped gap tuning curves and correct magnitude of gap thresholds are obtained by the model primarily because spike probability decreases as gap marker electrodes are separated. This results in larger standard deviation in the pdfs in the signal detection task, which in turn results in larger gap thresholds.

The number of fibres combined in a central detector and the electrode-nerve distance can be varied, but the model is not very sensitive to these parameters. The model suggests that variations in electrode-nerve distance may slightly skew the gap tuning curves, but is not as important as current distribution. This statement is based on the assumption that fibres are excited at a fixed threshold. However, the model of Hanekom (2001) shows that apparent fibre thresholds change considerably when electrodes are placed close to the modiolus.

The model suggests that the major factor determining the gap threshold tuning curve shapes is the current distribution, which depends on electrode design and cochlear impedance characteristics. Exponential current decay at different rates can control the slopes of the gap tuning curve flanks. Other irregular current distributions can predict the jagged shape of the gap tuning curves.

Neural parameters (threshold and RS) can be varied and, as has been shown, the variability of these can also predict the non-monotonic shape of the gap tuning curves. RS controls the slope of the gap tuning curve flanks. Finally, stimulation parameters (intensity of stimulation, pulse width, and frequency of stimulation) can be varied. The magnitude as well as the shape of predicted gap thresholds is sensitive to the intensity of stimulation.

4.5 Strengths and weaknesses of the current model

4.5.1 Strengths

As far as is known, this is the first model for gap detection in electric hearing. The model provides a simple explanation for gap detection thresholds as measured in cochlear implantees, using realistic model parameters. Gap detection threshold magnitudes are correct, and the U-shaped curves can be predicted. It is based on simple signal detection theory considerations. The model implementation performs analytical calculations and does not require lengthy Monte Carlo simulations.

The model also provides estimates of the current distributions based on psychophysical gap

detection data. Hence, current distributions may be estimated non-invasively. Evaluating whether the predicted current distributions are a fair reflection of the actual current distributions is impossible with currently available techniques. Tank measurements (Black et al., 1983) show similar trends than observed in the model predictions. If it can be proven that these predictions are good estimates of the actual current distributions, the model will be a particularly useful tool to individualise settings in cochlear implant programming.

4.5.2 Weaknesses

Three important criticisms of the current model are discussed here. First, a primary model assumption is that a limited extent observation (or attention) window is employed by the central gap detection mechanism. Not enough neurophysiological evidence is available to support this assumption. In fact, gap detection studies in normal acoustic hearing have shown that gap detection improves when the gap is present in more neural channels (Hall et al., 1996), although a similar result was not obtained in cochlear implantees in the study by Van Wieringen and Wouters, 1999.

Second, model assumptions about the neural spike train may be an oversimplification. It is assumed that only the *A* response occurs, while the *B* and *C* responses may also occur and complicate the central gap detector's task. However, it is believed that for modelling purposes it is reasonable to assume that only the *A* response occurs, as this response is predominant in long-term deaf ears. Occurrence of multiple spikes with different latencies in response to an electrical stimulus pulse will complicate the task of the central detector and makes it difficult to obtain model predictions for gap thresholds without reverting to Monte Carlo modelling. Creating such a model is possible. However, conceptually these multiple spikes just decrease the signal to noise ratio (i.e. they "fill the gap"), so that gaps become more difficult to detect and gap thresholds increase.

Finally, the signal detection calculations were based on gamma functions that approximated the multi-mode inter-spike interval histograms. This was to simplify calculations, but will influence the predicted gap thresholds.

4.5.3 Other arguments against the model

Chatterjee et al. (1998) and Van Wieringen and Wouters (1999) have argued against the notion that U-shaped gap detection curves originate from an across-channel gap detection mechanism where smaller neural overlap leads to increased gap thresholds.

One argument was that the same U-shaped curves can also be obtained with within-channel gap detection by either using markers with different stimulation pulse rate or intensity of stimulation (Chatterjee et al., 1998). This result will also be obtained with the current model. Although no calculations have been made, it is conceptually easy to see that the signal detection task is complicated by markers that differ in frequency, as gap detection is based on inter-spike interval duration. In the model, the gap detection mechanism searches for a change in inter-spike interval duration and detects a gap when this occurs. Inter-spike intervals that change without a gap occurring, confounds the gap detection mechanism, which will result in increased gap thresholds. So, although Chatterjee et al. (1998) are correct to suggest that within-channel processes can also result in U-shaped gap tuning curves, this does not negate the current model.

The role of perceptual dissimilarity processes cannot be precluded. U-shaped gap tuning curves obtained with differences in marker loudness (Chatterjee et al., 1998) are explained more easily by perceptual dissimilarity than by the current model. Van Wieringen and Wouters (1999) also argued that perceptual processes probably determine gap thresholds. A strong argument by these authors was that training eliminated the increase in gap thresholds in across-channel conditions in some subjects.

4.6 Future improvements of the model

One model limitation is the way that information is combined across a number of fibres that carry information about the gap. It has been assumed that spike train information from one critical band is combined to obtain predictions of gap thresholds. Under the (valid) assumption that these spike trains are very similar, the model simply calculates what the improvement in

signal-to-noise ratio is, and predicts gap thresholds under the assumption that spike trains are observed by a classical detector.

The model does not take into account that spike trains from widely-spaced positions in the cochlea may be combined to obtain predictions for gap thresholds. One future improvement will be that the model will incorporate mechanisms to combine non-similar spike trains from more widely-spaced positions.

Also, the model provides no *implementation* for the detection mechanism, but employs a *statistical* approach based on classical detection theory to provide gap threshold predictions. The model currently does not allow one to have a set of (simulated) spike trains containing the gap as input to a gap detection mechanism, which then has to detect the gap. Bayesian (as opposed to classical) estimation techniques, which employ an internal model of the signal to be detected, are explored in chapter 5 (for frequency discrimination). Chapters 5 to 7 explore the implementation-driven modelling approach, rather than the statistical approach used in this chapter and in chapter 3, by which an implementation for an optimal detector is devised. Such a detector can then use simulated spike trains as input and predictions can be derived with Monte Carlo simulation. The advantage of this approach is that complexities in spike trains (e.g. multiple spikes with multiple latencies) can be investigated.

Finally, the model takes only spatial, and not temporal, information into account. Decay of spike rate does not occur in cochlear electrical stimulation as in acoustic gap detection, but spike latencies are also not taken into account. Furthermore, adaptation and bursting (Shepherd and Javel, 1997) are not taken into account. All these complexities can be incorporated into an implementation-driven model.

5 CONCLUSION

A number of conclusions may be drawn from the modelling exercise in this chapter.

(1) Obtaining realistic gap detection thresholds in electric hearing by a spatial model that

does not allow for temporal models of gap detection is possible.

(2) Predictions for the current distribution in the cochlea of a specific implant user can be obtained from the gap detection tuning curves. It is not known how accurate these predictions are, but they do show trends similar to those found in current distribution measurements.

(3) The sharp tip seen in some gap tuning curves is possibly obtained when entrainment is close to 100%, when the primary factor determining gap thresholds is probably the temporal dispersion of spike placement in response to a stimulus pulse.

(4) The shallow bowl portion of the gap tuning curve is probably obtained when entrainment is not close to 100%, when gap thresholds are probably determined by standard deviation of the inter-spike interval pdf.

(5) Electrode array placement relative to the neural plane plays a secondary role in determining gap thresholds.

(6) The primary factor determining gap thresholds is probably the shape of the current distribution. Modelling results suggest that exponential current decay is not a good model of current distribution in the cochlea. Possibly, for bipolar stimulation, sharper current peaks are obtained close to the electrode.

(7) The model rests on the important assumptions that an attention window or observation window exists, that this window is placed for optimal gap detection probability, and that the gap detection mechanism uses spike train information from this window exclusively. This assumption cannot be proven or disproven by the current model.

APPENDIX 4.A

Equation 4.14 is a polynomial that was fit to obtain the required b values for values of σ_r between 2 ms and 100 ms. The coefficients in this equation are $p_1 = -5.2745 \times 10^{-12}$, $p_2 = 2.1284 \times 10^{-9}$, $p_3 = -3.5133 \times 10^{-9}$, $p_4 = 3.0544 \times 10^{-5}$, $p_5 = -0.0015$, $p_6 = 0.0416$, $p_7 = -0.6214$ and $p_8 = 5.8933$.

The definitions of the gamma function $\Gamma(b)$ and incomplete gamma function $\Gamma(b,a)$ as used in chapter 4 are given in equations 4.A.1 and 4.A.2.

$$\Gamma(b) = \int_0^\infty t^{b-1} e^{-t} dt \tag{4.A.1}$$

$$\Gamma(b,a) = \int_a^\infty t^{b-a} e^{-t} dt \tag{4.A.2}$$